Computers and Chemical Engineering 200 (2025) 109167

Contents lists available at ScienceDirect

Computers and Chemical Engineering

journal homepage: www.elsevier.com/locate/compchemeng

Dyn2Heat – MILP Heat Exchanger Network Design for Batch Processes via Dynamic Optimization

Dörthe Franzisca Hagedorn, Laura Kuper, Mats Zoellmann, Christiane Reinert, Niklas von der Assen *

Institute of Technical Thermodynamics, RWTH Aachen University, Schinkelstr. 8, 52062 Aachen, Germany

ARTICLE INFO

Keywords:
Energy Efficiency
Heat Integration
Pinch Method
Logarithmic Mean Temperature Difference
Dynamic Processes
Ordinary Differential Equations

ABSTRACT

Nowadays, the energy efficiency of batch processes is getting increasing attention. Heat integration is an established approach to increase energy efficiency. However, compared to continuous processes, the temporally dynamic behaviour of batch processes introduces additional complexity to the heat exchanger network design problem. Furthermore, including investment costs of heat exchangers in the economic optimization problem requires spatial modelling of the heat exchangers. The spatial modelling usually leads to nonlinearities, which can lead to computational intractability. In our work, we demonstrate that both, the temporal and the spatial temperature profiles in a heat exchanger network for batch processes, can be modelled efficiently by differential equations. We introduce the Dyn2Heat model, a dynamic optimization model for heat exchanger network design for batch processes. The Dyn2Heat model considers the economic trade-off between process duration, investment costs for heat exchangers and operational costs for utility supply. At the same time, the dynamic formulation makes the model computationally efficient in comparison to a nonlinear algebraic formulation and applicable to complex systems involving several possible heat exchangers.

1. Introduction to Heat Exchanger Network Design in Batch Processes

Currently, climate change and rising energy cost necessitate energy efficiency in industrial processes. Industrial heating causes around a quarter of the global final energy consumption (International Energy Agency, 2022). The industrial heating demand can be reduced by heat integration. Heat integration can be defined as reusing waste heat of a certain process as a heat source for another process in the same industrial side. Thus, heat integration can reduce both, the heating and cooling demand at the same time. The most established method in the field of heat integration is the pinch analysis originally introduced by Linhoff and Flower (1978). Refer to (Klemeš and Kravanja, 2013; Linnhoff and Flower, 1978) and (Kemp and Lim, 2020) for further information on pinch analysis and heat integration.

Pinch analysis is well suited to derive the thermodynamic potential for heat integration. However, to implement heat integration in practice, a heat exchanger network needs to be designed. For the heat exchanger network design (HEND) task, pinch analysis uses some heuristics, not necessarily leading to the optimal heat exchanger network configuration. Thus, some superstructure-based optimization models have been proposed to mathematically optimize the heat exchanger network design. One of the most established optimization models for heat exchanger network design is the so-called Synheat model by Yee and Grossmann (1990) which is based on a stage-wise superstructure.

The original Synheat model concentrates on continuous processes. Compared to continuous processes, heat integration for batch processes has been neglected (Fernández et al., 2012). Nowadays, batch processes are getting more and more important as they are essential to produce high-value products. Batch processes are implemented for example in the chemical, pharmaceutical and food industry as batch processes offer more flexibility and adaptability than continuous processes.

At the same time, batch processes are more complex to operate and to design due to their non-stationary behavior. Regardless, some approaches still consider batch processes in heat exchanger network design. Following the approach of pinch analysis, Kemp and Deakin (Kemp and Deakin, 1989a) introduce the cascade analysis to consider batch processes in heat integration problems. In a time slice model (TSM), they divide the process into different time intervals to take the time-dependency of batch processes into account. The authors analyze

* Corresponding author.
E-mail address: niklas.vonderassen@ltt.rwth-aachen.de (N. von der Assen).

https://doi.org/10.1016/j.compchemeng.2025.109167
Received 19 April 2024; Received in revised form 8 April 2025; Accepted 29 April 2025
Available online 2 May 2025
0098-1354/© 2025 The Author(s). Published by Elsevier Ltd. This is an open access article under the CC BY license (http://creativecommons.org/licenses/by/4.0/).

the design of heat exchanger networks based on the TSM and the influence of storages and rescheduling in the second part of the three-paper series (Kemp and Deakin, 1989b). However, the approach is based on the pinch analysis and includes some heuristics and the authors conclude that the design of heat exchanger networks for batch processes is tedious. Zhao et al. (Zhao et al., 1998) introduce a three-step procedure for the heat exchanger network design in batch processes. The procedure is built upon the TSM. The first step are individual heat exchanger network designs for each timestep, which are then combined to one cost effective common network by rematching heat exchangers between the different time slices. However, the method builds upon the pinch analysis and cannot guarantee a cost optimum.

Aaltola (2002) and Verheyen and Zhang (2006) extend the original Synheat model (Yee and Grossmann, 1990) for multi-period processes with quasi-stationary behavior in each time step. However, quasi-stationary behavior cannot be assumed for most batch processes, like heating or cooling in vessels. Such processes with temporally dynamic behavior induce a new complexity to the heat integration problem due to their temporal temperature profiles.

Already in 1944, Fisher described the problem of heating or cooling of a vessel by an external heat exchanger and derived an expression to describe the resulting temperature profiles (Fisher, 1944). Later, Vaselenak et al. (1986) published one of the first methods for heat integration in batch processes considering temporal temperature profiles. The authors regard three different settings of vessels and heat exchangers and draw an analogy to counter-current and co-current heat transfer. Their method predicts the maximum possible heat integration for each setting. Furthermore, they introduce a heuristic and a mixed-integer linear optimization problem to derive which vessels should be heat integrated, if there are more than two vessels involved in the problem. The authors note that the process duration depends on parameters such as the heat exchanger area or the minimum temperature difference between the integrated fluids, which are subject to the design of the process. However, processing time is not directly considered in the study.

Boyadjiev et al. (1996) solve the problem of optimal heat integration for a real-world case study of a batch antibiotics manufacture by focusing on two problems: the optimal operation and the scheduling. For the optimal operation, they formulate an optimal control problem in the form of a dynamic optimization problem to minimize the overall external utility costs. In their formulation, the process duration is a variable and determined by optimization, as the heat integration influences the necessary operation time. However, the structure of the heat exchanger network and the size of the heat exchangers is predetermined.

In their two-paper series, Ivanov and co-workers formulate the problem of optimizing the heat exchanger sizes and mass-flow rates for a heat integrated two-vessel batch problem with simultaneous utility supply in a given time interval without (Ivanov et al., 1992) and with (Peneva et al., 1992) the usage of a heat transfer medium. Later, Vaklieva-Bancheva extends the models of Ivanov et al. (1992) and Peneva et al. (1992) for indirect heat integration, i.e. for the inclusion of thermal storages (Vaklieva-Bancheva, 2022). The author underlines the complexity of heat integration in batch processes and concludes that the design of heat exchanger networks for batch processes requires systematic non-traditional methods for global optimization.

Dowidat et al. (2014) derive a scheme to prepare dynamic processes for the use in the time slice model by linearizing the dynamic temperature profile. However, no general statement on the accuracy of the linearization in (Dowidat et al., 2014) compared to the real dynamic behavior can be made.

Castro (2016) links the temperature stages of the Synheat model to time points to represent batch processes in the Synheat model. They solve the heat integration problem simultaneously to the scheduling of the process. For the temporal temperature profiles, they use linear ramping constraints to limit the rate of temperature change over time.

However, in all the methods mentioned before, investment costs for heat exchangers are neglected. Instead, most approaches optimize the number of matches, but no heat exchanger sizing is carried out. Thus, the thermodynamic potential for heat integration can be optimized, but the cost-optimum for the implementation of heat integration by a heat exchanger network cannot be guaranteed.

To optimize the total costs comprising investment costs for heat exchangers and operational costs for external utilities, the heat exchanger network design problem needs to be solved. Recently, we introduced the DynHeat model for heat exchanger network design in batch processes at the ESCAPE conference 33 (Hagedorn et al., 2023). We could show that a dynamic optimization model is suitable for the modeling of batch processes in HEND problems. Furthermore, we could show that there is a trade-off between the total costs for the process and the process duration which can be addressed by multi-objective optimization. To the best of our knowledge, the model was the first model for HEND in batch processes with explicit modelling of the dynamic temperature profiles as differential equations. However, as most existing HEND models, the DynHeat model includes the strongly nonlinear logarithmic mean temperature difference (LMTD) to model the spatial temperature profiles in the heat exchangers and is therefore hard to solve by off-the-shelf solvers.

Because of the numerical complexity, instead of using the LMTD function, some alternative approximations have been introduced, as for example the Chen approximation (Chen, 1987) or the Paterson approximation (Paterson, 1984). However, the approximations are still nonlinear functions and as approximations, they do not represent the actual temperature profiles exactly. Thus, some research on the LMTD function itself has been performed. Chen (2019) proposes an explicit solution to the LMTD function by using the Lambert *W*-function. Mistry and Misener (2016) analyze the properties of the LMTD function. They could proof convex behavior under specific circumstances. The convexity offers the possibility to handle the LMTD function more efficiently in decomposition approaches like outer approximation. The authors also propose an efficient solution algorithm based on their analysis for the Synheat problem. Huang et al. (2012) and Kazi et al. (2021b) use a robust reformulation of the LMTD function by adding a small value to eliminate the non-smooth behavior of the LMTD.

However, instead of using the algebraic LMTD function as a solution to the differential equations, the temperature profiles in a heat exchanger can also be modeled by the spatial differential equations directly in a dynamic optimization problem. This approach of using spatial differential equations for the design of heat exchangers was used by Kazi et al. (2021a) for detailed design of shell and tube heat exchangers. For discrete decisions, the authors iteratively solve a purely algebraic model, based on the LMTD function, as they avoid incorporating integer variables into the dynamic problem. However, in our former work (Hagedorn et al., 2023), we could show that a dynamic optimization problem including integer variables is a promising approach for HEND in batch processes that can be solved by direct transcription based on orthogonal collocation on finite elements.

All in all, dynamic optimization models can model the dynamic behavior of batch processes more precisely compared to linear approximations and have the potential to be more efficient than nonlinear algebraic approaches. At the same time, dynamic optimization models can model the spatial temperature profiles in heat exchangers computationally efficiently as compared to algebraic models including the LMTD function and its approximations. Thus, a dynamic optimization model is a promising approach for HEND in batch processes. To the best of our knowledge, no such dynamic optimization model for HEND in batch processes that can efficiently model the trade-off between investment costs for heat exchangers, the utility costs, and the process duration, exists so far.

In this work, we introduce the Dyn2Heat model, a dynamic optimization model for HEND in batch processes. The Dyn2Heat model extends our DynHeat model (Hagedorn et al., 2023) by spatial differential equations instead of using the LMTD function. Thus, the Dyn2Heat

model includes both, spatial and temporal differential equations to model the temperature profiles.

We solve the mixed-integer dynamic optimization problem by discretizing the model based on orthogonal collocation on finite elements (Biegler, 2010; Nicholson et al., 2018). The resulting discretized problem is a mixed-integer linear problem, which makes the model easier to solve compared to our formerly presented nonlinear DynHeat model. Furthermore, we introduce an iterative method to refine the step size for the discretization in the surrounding of the optimum, balancing the trade-off between accuracy and number of integer variables.

The remainder of this paper is structured as follows: In the next section, we will introduce the Dyn2Heat model by giving the problem statement and deriving the central differential equations before defining the optimization model in detail. Furthermore, we will introduce the applied solution scheme of direct transcription based on orthogonal collocation and describe the iterative refinement method for improved discretization. Afterwards, we will apply the Dyn2Heat model to a simplified case study and evaluate its performance in comparison to a fully algebraic model formulation. To proof the performance of the Dyn2Heat model for more complex structures, we will then apply the Dyn2Heat model to a second case study and evaluate the results. Finally, we will conclude our work and give an outlook on relevant topics for future works.

2. Method: The Dyn2Heat Model for Heat Exchanger Network Design in Batch Processes

2.1. Introduction to the Dyn2Heat Model

This work introduces the Dyn2Heat model for optimal heat integration in batch processes with dynamic temperature profiles, i.e., heating and cooling in vessels. To implement heat integration in such batch processes in an economically efficient way, heat exchanger networks need to be designed and operation needs to be optimized. In the Dyn2Heat model, we assume sequential operation, i.e., first the optional heat integration will be used and afterwards the remaining heating and cooling demand will be supplied by utility. The operational optimization defines the optimal duration of the process: the longer heat integration is performed, the less utility must be supplied, resulting in lower operational costs. On the other hand, a longer process duration can be undesirable as it may reduce the throughput of the process. Thus, there is a trade-off between process duration and utility costs that needs to be addressed by the optimization model, as shown by (Hagedorn et al., 2023). Furthermore, there is a trade-off with the investment costs for heat exchangers: Larger heat exchangers lead to a higher heating and cooling power. Thus, larger heat exchangers lead to quicker heat integration and utility supply and can reduce the process duration as well. However, bigger heat exchangers also lead to higher investment costs. Thus, deriving the optimal heat exchanger network design and operation for heat integrated batch processes is a complex task that can be addressed by mathematical optimization.

To optimize the operation, temporal temperature profiles of the involved media must be modeled in the optimization model. Furthermore, to assess the optimal size of a heat exchanger, the spatial temperature profile within the heat exchanger must be modeled. Fig. 1 shows an exemplary heat exchanger connecting one hot and one cold vessel. The spatial temperature profile along the heat exchanger surface area a^{HI} and the temporal temperature profile in the heat exchanger along the time axis t^{HI} result in a double logarithmic temperature profile (Glück, 2017). Such a double logarithmic temperature profile is qualitatively shown in Fig. 1. Instead of using the algebraic double-logarithmic mean function, we use spatial and temporal differential equations to model the temperature profiles in the dynamic optimization model, the Dyn2Heat model, efficiently.

In the following section, we present the problem statement for the

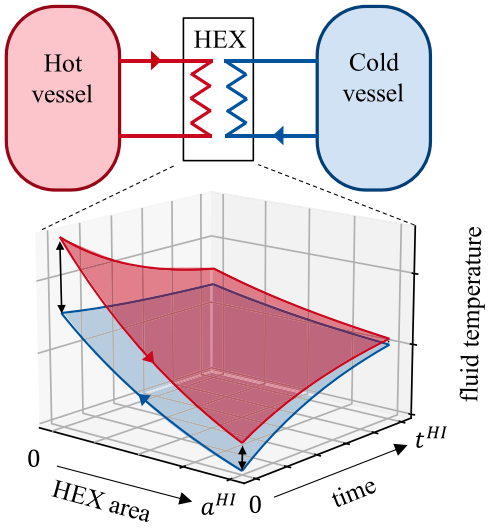


Fig. 1. The graphic shows exemplarily a counter-current heat exchanger (HEX) between a hot vessel (left, red) that is cooled down and a cold vessel (right, blue) that is heated up. Heat integration between these two vessels results in a double logarithmic temperature profile in the dimensions of the heat exchanger surface area a^{HI} and the time t^{HI}.

Dyn2Heat model before we describe the central differential equations and derive the ordinary form that we use in the model. Afterwards, we define the mathematical model. We describe the most relevant model constraints and the objective function. To solve the model, we use a discretization method based on orthogonal collocation on finite elements. After the model definition, we describe the solution approach and a refinement method to meet the trade-off between discretization accuracy and model size.

2.2. The Dyn2Heat Problem Statement

In the following section, we define the Dyn2Heat problem statement. Fig. 2 shows the setup of the modeled batch process of two vessels, a hot vessel (left) that needs to be cooled and a cold vessel (right) that needs to be heated. In this work, we analyze the given setup for two vessels. In fact, the Dyn2Heat model can be extended to systems with more than two vessels as well. We assume that the vessels are perfectly mixed and thus each have a uniform, time-dependent temperature ($\boldsymbol{T_h^V}(t)$ and $\boldsymbol{T_c^V}(t)$). The vessels can be provided with heating and cooling from external utilities through dedicated heat exchangers (Ut). Furthermore, there is an option to install an external heat exchanger (HI) to integrate heat between the vessels. For the heat transfer, either for heat integration or for utility supply, a heat transfer medium (HTM) is used on both sides. We assume sequential operation, i.e., the heat integration will always finish before the utility supply starts. To allow for this sequential operation, the operation mode can switch from heat integration to utility supply by directing the HTM through the respective heat exchangers by three-way valves. We assume that the same heat transfer medium is used for both operation modes in this work. However, the modular structure of the Dyn2Heat model would also allow for different transfer media for both operation modes.

We define the problem statement as follows:
Given:

- Hot vessels $h \in H$ and cold vessels $c \in C$ with their respective mass (m_h^V, m_c^V), heat capacity ($c_{p,h}$, $c_{p,c}$), start and target temperatures ($T_h^{V,\,start}$, $T_c^{V,start}$, $T_h^{V,\,target}$, $T_c^{V,target}$).
- The mass flow rates of the heat transfer media in the vessels ($\dot{m}_h^{HTM}$, $\dot{m}_c^{HTM}$) and in the external heat exchangers ($\dot{m}_m^{HI,hot}$, $\dot{m}_m^{HI,cold}$) and the

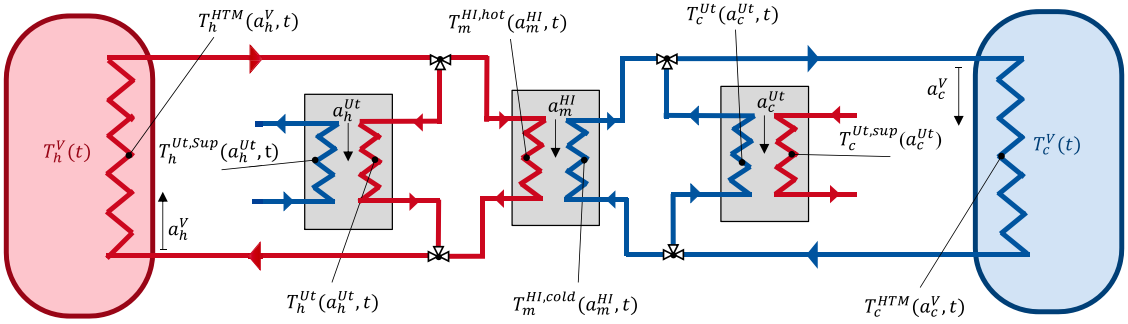


Fig. 2. Scheme of a batch process with one hot vessel (left, red) and one cold vessel (right, blue). An optional external heat exchanger (middle grey box) allows for heat integration (HI) between the two vessels. Furthermore, the two vessels can be provided with heating and cooling from external utility (Ut) through additional dedicated heat exchangers (left grey box and right grey box, respectively). A heat transfer medium (HTM) is used for the heat transfer. The operation mode can switch from heat integration to utility supply by directing the HTM through the respective heat exchangers (the respective three-way valves are depicted as white triangles). The Dyn2Heat model can design the heat exchanger network and optimize the operation of such a heat integrated batch process.

respective heat capacities of the heat transfer media ($c_{p,h}^{HTM}$, $c_{p,c}^{HTM}$, $c_{p,m}^{HI,hot}$, $c_{p,m}^{HI,cold}$).
- The heat transfer coefficient of the optional heat exchangers (k).
- Economic parameters as utility costs ($cost^{HU}$, $cost^{CU}$) and specific costs for the heat exchangers ($cost^{HEX,init}$, $cost^{HEX,A}$) and an optional time penalty in form of specific time costs ($cost^{t}$).
- Inlet temperatures ($T_h^{Ut,sup,0}$, $T_c^{Ut,sup,0}$), mass flow rates ($\dot{m}_h^{Ut}, \dot{m}_c^{Ut}$) and heat capacities ($c_{p,c}^{Ut}$, $c_{p,h}^{Ut}$) of the external utilities.
- The number of batches per year N^b to relate the annualized investment costs to one batch.

The possible matches $m \in M$ for heat integration between the vessels, i.e. which hot vessel can potentially be connected to which cold vessel via an external heat exchanger. Note that we analyse the setup for two vessels in this work. Although the presented Dyn2Heat model formulation does not include a generalized superstructure formulation, the modular formulation of the Dyn2Heat model allows for adaption to different superstructures. The superstructure of the possible heat exchanger network, i.e., the possible matches $m \in M$, is predefined by matching the temperatures of the heat transfer media accordingly by equality constraints. For the setup shown in Fig. 2, the matching equality constraints are given in Appendix B (Eq. B26 a-f).

Find:

- The cost-optimal heat exchanger sizes ($\boldsymbol{A_m^{HI}}$, $\boldsymbol{A_c^{Ut}}$, $\boldsymbol{A_h^{Ut}}$, $\boldsymbol{A_h^V}$, $\boldsymbol{A_c^V}$) and process operation by minimizing the total costs comprising investment costs for the heat exchangers related to one batch run, operational costs for utility supply and an optional time penalty for the duration of the process. The optimal operation includes the heating and cooling supplied by utility ($\boldsymbol{Q_c^{Ut}}$, $\boldsymbol{Q_h^{Ut}}$), the process duration for heat integration and of the whole process ($\boldsymbol{dur^{HI}}, \boldsymbol{dur}$) and the resulting optimal temperature profiles of all media, i.e. of the vessel fluids ($\boldsymbol{T_h^V}(t)$, $\boldsymbol{T_c^V}(t)$), of the utilities ($\boldsymbol{T_h^{Ut,sup}}(a_h^{Ut},t), \boldsymbol{T_c^{Ut,sup}}(a_c^{Ut},t)$), and of the heat transfer media in all heat exchangers ($\boldsymbol{T_m^{HI,hot}}(a_m^{HI},t)$, $\boldsymbol{T_m^{HI,cold}}(a_m^{HI},t)$, $\boldsymbol{T_h^{HTM}}(a_h^V,t)$, $\boldsymbol{T_c^{HTM}}(a_c^V,t)$, $\boldsymbol{T_h^{Ut}}(a_h^{Ut},t)$, $\boldsymbol{T_c^{Ut}}(a_c^{Ut},t)$). Here, t denotes the continuous time domain and a_h^{Ut}, a_c^{Ut}, a_m^{HI}, a_h^V and a_c^V denote the continuous spatial domains of the respective heat exchangers.

Assumptions:

- Sequential operation, i.e., first heat integration occurs, afterwards the remaining demands are supplied by external utilities.
- Perfect mixture in the vessels, i.e., the fluid temperature in the vessels is uniform.
- Constant specific heat capacities of all fluids and constant heat transfer coefficients of all heat exchangers.
- Only sensible heating and cooling, no reaction or phase changes occur.
- No heat losses.
- Thermal inertia of the heat exchangers is neglected, i.e., heat exchanger walls cannot store heat and react immediately to an imposed temperature change.
- One-by-one matches between hot and cold vessels, i.e., each cold vessel can only be connected to one dedicated hot vessel and vice-versa.

2.3. Differential equations for the temperature profiles

Before we present the mathematical model, we derive the differential equations to model the temperature profiles, as the key model equations first. We explain the differential equation for the temperature at the cold side of the external heat exchanger in Fig. 2 ($\boldsymbol{T_m^{HI,cold}}(a_m^{HI},t)$) and simplify the partial differential equation to an ordinary differential equation (ODE). Other differential equations of the model can be derived analogously.

The partial differential equation for the temperature at the cold side of the counter-current external heat exchanger is given in Equation (1), analogously to (Maidi et al., 2009)

$$\underbrace{\frac{\partial \boldsymbol{T_m^{HI,cold}}(z_m^{HI},t)}{\partial t}}_{\text{temporal term}} + \underbrace{v_m^{HI,cold} \cdot \frac{\partial \boldsymbol{T_m^{HI,cold}}(z_m^{HI},t)}{\partial z_m^{HI}}}_{\text{spatial term}} = \underbrace{\frac{k \cdot a_m^{HI,cold}}{\rho_m^{HI,cold} \, c_{p,m}^{HI,cold} \cdot S_m^{HI,cold}} \cdot \left(\boldsymbol{T_m^{HI,hot}}(z_m^{HI},t) - \boldsymbol{T_m^{HI,cold}}(z_m^{HI},t)\right)}_{\text{heat transfer between the fluids}} \tag{1}$$

with the fluid velocity of the cold fluid $v_m^{HI,cold}$, the fluid density $\rho_m^{HI,\,cold}$, the heat capacity $c_{p,m}^{HI,\,cold}$, the heat transfer coefficient k, the heat exchange area per unit length a_m^{HI}, the cross-sectional area of the stream S_m^{HI} and the local current temperature of the hot-side fluid $\boldsymbol{T_m^{HI,hot}}(z_m^{HI},t)$. The coordinate z_m^{HI} denotes the flow axis along the heat exchanger and t the time. An analogous differential equation can be formulated for the hot side of the heat exchanger. This first-order hyperbolic partial differential equation system is commonly used in heat exchanger control problems, e.g. in (Hamze et al., 2018; Sano, 2021). However, this work does not intend to derive a detailed control strategy for heat exchangers. Instead, we intend to design the optimal heat exchanger network while considering the dynamics of the surrounding system.

We assume that the transient response of the heat exchanger is fast in comparison to the slower dynamics of the surrounding system. Slower dynamics of the surrounding system means that the temperatures in the

vessels change only slowly in comparison to the temperature change of the fluids along the heat exchanger. This assumption implies that the surrounding system imposes only small inlet temperature changes to the heat exchanger, and that these small changes are propagated through the whole heat exchanger almost immediately. As a result, the heat exchanger quickly returns to steady-state behaviour after small changes in the inlet temperature. Therefore, we assume a quasi steady-state temperature profile in the heat exchanger for each time point. This assumption is valid for high heat capacities of the vessels in comparison to the heat capacity flow rates multiplied by the dwell time in the heat exchanger, neglectable thermal capacity and thermal inertia of the heat exchanger walls and fast fluid velocities in the heat exchangers, which implies a sufficiently small ratio of $\frac{S_m^{HI}}{a_m^{HI}}$. We discuss this assumption in more detail in Appendix A. Ivanov et al., (1992) make a similar assumption by neglecting the transients of the heat exchanger. Under the assumption of quasi steady-state behaviour of the heat exchangers, we neglect the temporal derivative and transform eq. (1) to the ODE describing the steady-state heat balance of a heat exchanger:

$$\frac{\rho_m^{HI,cold}\cdot c_{p,m}^{HI,cold}\cdot S_m^{HI,cold}}{a_m^{HI,cold}}\cdot v_m^{HI,cold}\cdot\frac{d\boldsymbol{T_m^{HI,cold}}(z_m^{HI},t)}{dz_m} = k\cdot\left(\boldsymbol{T_m^{HI,\ hot}}(z_m^{HI},t)-\boldsymbol{T_m^{HI,cold}}(z_m^{HI},t)\right) \tag{2}$$

Note that the temperatures of the fluids in the heat exchangers are still a function of time, as the inlet temperature imposed by the surrounding system changes with time and the steady-state profile adapts to these changes. With the mass flow rate $\dot{m}_m^{HI,cold} = \rho_m^{HI,cold}\cdot S_m^{HI,cold}\cdot v_m^{HI,cold}$, equation (2) can be reformulated to:

$$c_{p,m}^{HI,cold}\cdot\frac{\dot{m}_m^{HI,cold}}{a_m^{HI,cold}}\cdot\frac{d\boldsymbol{T_m^{HI,cold}}(z_m^{HI},t)}{dz_m^{HI}} = k\cdot\left(\boldsymbol{T_m^{HI,\ hot}}(z_m^{HI},t)-\boldsymbol{T_m^{HI,cold}}(z_m^{HI},t)\right) \tag{3}$$

Furthermore, as done in (Kazi et al., 2021a), instead of the flow axis z_m^{HI}, we use the heat exchanger surface area a_m^{HI} as spatial coordinate with $da_m^{HI} = a_m^{HI}\cdot dz_m^{HI}$. With this change we receive the final form of the ODE:

$$-\dot{m}_m^{HI,cold}\cdot c_{p,m}^{HI,cold}\cdot\frac{d\boldsymbol{T_m^{HI,cold}}(a_m^{HI},t)}{da_m^{HI}} = k\cdot\left(\boldsymbol{T_m^{HI,hot}}(a_m^{HI},t)-\boldsymbol{T_m^{HI,cold}}(a_m^{HI},t)\right) \tag{4}$$

Note that the coordinate a_m^{HI} is defined in the opposite direction than the flow axis of the stream of the cold heat transfer medium (Fig. 2), which causes a minus on the left-hand side.

Equation (4) can be derived analogously for the hot side of the heat exchanger. Furthermore, the differential equations for the heat exchangers in the vessels and for the heat exchangers for utility supply follow the same differential equations. However, the differential equation further simplifies for these heat exchangers, as the vessel fluids are only time-dependent due to the perfect-mixture assumption and the inlet temperatures of the utilities are constant in time. In the Dyn2Heat model, the presented differential equations model the temperature profiles of the fluids along the heat exchangers and over time. The differential equations model a continuous temperature profile in the considered dimensions. However, the model must also allow for kinks in the temperature profile, when the end of the heat exchanger is reached or the operation mode of the process switches from heat integration to utility supply or to the finish. The switches require that the differential equations must only be active in a certain range of time and heat exchanger area. However, this range of validity for each differential equation is not predefined, as the heat exchanger areas and the duration of heat integration and of utility supply are subject to optimization. To activate the differential equations only for their respective range of validity, we introduce binary variables. For the regarded differential Eq. (4) the binaries are $x_m^{HI}(a_m^{HI})$ defined over the continuous spatial domain $a_m^{HI}\in[0:a^{MAX}]$ and $x_m^{t,HI}(t)$ defined over the continuous temporal domain $t\in[0:t^{MAX}]$. $x_m^{HI}(a_m^{HI})$ will have the value 1, when $0\le a_m^{HI}\le \boldsymbol{A_m^{HI}}$, i.e., when the spatial domain is within the heat exchanger surface area, and have the value 0 for all other values of a_m^{HI}. Analogously, x_{HI}^t will have the value 1 for $0\le t\le \boldsymbol{dur^{HI}}$, i.e., as long as heat integration occurs. With the binaries, the ODE for the cold side of an external heat exchanger Eq. (4) becomes:

$$\begin{aligned}&\dot{m}_m^{HI,cold}\cdot c_{p,m}^{HI,cold}\cdot\frac{d\boldsymbol{T_m^{HI,cold}}(a_m^{HI},t)}{da_m^{HI}}\\ &= \boldsymbol{x_m^{HI}}(a_m^{HI})\cdot\boldsymbol{x_m^{t,HI}}(t)\cdot k\cdot\left(\boldsymbol{T_m^{HI,cold}}(a_m^{HI},t)-\boldsymbol{T_m^{HI,hot}}(a_m^{HI},t)\right)\\ &\forall\ m\in M\end{aligned} \tag{5}$$

We reformulate the nonlinear product of binaries and continuous variables on the right-hand side by a big-M formulation, leading to the following set of constraints:

$$\begin{aligned}&\frac{\dot{m}_m^{HI,cold}\cdot c_{p,m}^{HI,cold}}{k}\cdot\frac{d\boldsymbol{T_m^{HI,cold}}(a_m^{HI},t)}{da_m^{HI}}-\left(\boldsymbol{T_m^{HI,cold}}(a_m^{HI},t)-\boldsymbol{T_m^{HI,hot}}(a_m^{HI},t)\right)\\ &\le\left(1-\boldsymbol{x_m^{HI}}(a_m^{HI})\right)\cdot M+\left(1-\boldsymbol{x_m^{t,HI}}(t)\right)\cdot M\\ &\forall\ m\in M\end{aligned} \tag{6a}$$

$$\begin{aligned}&\frac{\dot{m}_m^{HI,cold}\cdot c_{p,m}^{HI,cold}}{k}\cdot\frac{d\boldsymbol{T_m^{HI,cold}}(a_m^{HI},t)}{da_m^{HI}}-\left(\boldsymbol{T_m^{HI,cold}}(a_m^{HI},t)-\boldsymbol{T_m^{HI,hot}}(a_m^{HI},t)\right)\\ &\ge-\left(1-\boldsymbol{x_m^{HI}}(a_m^{HI})\right)\cdot M-\left(1-\boldsymbol{x_m^{t,HI}}(t)\right)\cdot M\\ &\forall\ m\in M\end{aligned} \tag{6b}$$

$$\frac{d\boldsymbol{T_m^{HI,cold}}(a_m^{HI},t)}{da_m^{HI}}\le\boldsymbol{x_m^{HI}}(a_m^{HI})\cdot M\qquad\forall m\in M \tag{6c}$$

$$\frac{d\boldsymbol{T_m^{HI,cold}}(a_m^{HI},t)}{da_m^{HI}}\ge-\boldsymbol{x_m^{HI}}(a_m^{HI})\cdot M\quad\forall m\in M \tag{6d}$$

$$\frac{d\boldsymbol{T_m^{HI,cold}}(a_m^{HI},t)}{da_m^{HI}}\le\boldsymbol{x_m^{t,HI}}(t)\cdot M\qquad\forall m\in M \tag{6e}$$

$$\frac{d\boldsymbol{T_m^{HI,cold}}(a_m^{HI},t)}{da_m^{HI}}\ge-\boldsymbol{x_m^{t,HI}}(t)\cdot M\quad\forall m\in M \tag{6f}$$

Eq. (6a) and Eq. (6b) ensure that the differential equation is active, i.e., fulfilled exactly, when both binaries take the value 1. Eq. (6c) – Eq. (6f) ensure that the derivative of the temperature with respect to the heat exchanger area is 0, if either of the binaries is zero, i.e., the equations ensure that no temperature change occurs outside the heat exchanger or when no heat integration takes place. An equivalent big-M reformulation is used for all other differential equations with binary variables.

2.4. Dyn2Heat Model Definition

In the following, we present the Dyn2Heat model definition. We define the objective function of the model and the model constraints, including the ODE derived above. We focus on the central model equations, whereas the full model is given in Appendix B. To improve readability, we will note all optimization variables in bold letters.

The objective of the Dyn2Heat model is the minimization of the total costs for one batch run, comprising operational costs $\boldsymbol{cost^{operation,total}}$ and investment costs $\boldsymbol{cost^{invest,total}}$ for heat exchangers related to one batch run by dividing the annualized investment costs by the number of batches per year N^{batch}. Note that the process duration itself may influence the number of batches per year. However, in this work, we assume that the number of batches is fixed and given as a parameter. The total costs depend on the surface area of the different heat exchangers, the energy supplied by hot utility $\boldsymbol{Q_c^{Ut}}$ and cold utility $\boldsymbol{Q_h^{Ut}}$ to meet the

heating and cooling demands of each cold vessel $c \in C$ or hot vessel $h \in H$, and on the duration of the process ***dur***. The heat exchangers include the external heat exchangers for heat integration with the area $\boldsymbol{A_m^{HI}}$ for each possible match $m \in M$ between a hot and a cold vessel, the heat exchangers in the vessels with the respective areas $\boldsymbol{A_h^V}$ and $\boldsymbol{A_c^V}$, and the heat exchangers for utility supply with the respective areas $\boldsymbol{A_h^{Ut}}$ and $\boldsymbol{A_c^{Ut}}$.

$$\min_{\left\{A_m^{HI},\ A_h^{Ut}, A_c^{Ut},\ A_h^V, A_c^V, Q_c^{Ut},\ Q_h^{Ut},\ dur\right\}} f\left(\boldsymbol{A_m^{HI}},\ \boldsymbol{A_h^{Ut}}, \boldsymbol{A_c^{Ut}},\ \boldsymbol{A_h^V}, \boldsymbol{A_c^V}, \boldsymbol{Q_c^{Ut}},\ \boldsymbol{Q_h^{Ut}},\ \boldsymbol{dur}\right) = \frac{\boldsymbol{cost^{invest,total}}}{N^{batch}} + \boldsymbol{cost^{operation,total}} \tag{7}$$

In this work, we assume that the investment costs depend linearly on the heat exchanger surface areas. The linear investment costs comprise costs proportional to the heat exchanger surface areas with the cost factor $cost^{HEX,A}$ and initial costs $cost^{HEX,init}$ describing fixed base costs that may occur if a heat exchanger is built. The specific cost factors $cost^{HEX,init}$ and $cost^{HEX,A}$ are predefined as parameters. The binary variables $x^{HEX}(a^{HEX})$ defined over the spatial domain of each heat exchanger a^{HEX} indicate that a heat exchanger is built, if they have the value 1 for $(a^{HEX} = 0)$.

$$\boldsymbol{cost^{invest,\ total}} = cost^{HEX,init} \cdot \left(\sum_{m \in M} \boldsymbol{x_m^{HI}}(0) + \sum_{h \in H} \left(\boldsymbol{x_h^V}(0) + \boldsymbol{x_h^{Ut}}(0)\right) + \sum_{c \in C} \left(\boldsymbol{x_c^V}(0) + \boldsymbol{x_c^{Ut}}(0)\right) \right) + cost^{HEX,A} \cdot \left(\sum_{m \in \boldsymbol{M}} \boldsymbol{A_m^{HI}} + \sum_{\boldsymbol{h} \in \boldsymbol{H}} \left(\boldsymbol{A_h^{Ut}} + \boldsymbol{A_h^V}\right) + \sum_{c \in C} \left(\boldsymbol{A_c^{Ut}} + \boldsymbol{A_c^V}\right) \right) \tag{8}$$

The linear dependency of the investment costs used in this work is a simplified assumption. It is possible to include a more sophisticated cost model into the objective function, e.g. economy of scale by adding a cost exponent. However, a more sophisticated cost function might lead to nonlinearities in the objective function and, thus, change the problem class of the model. If a nonlinear objective function is used, linearization techniques such as piecewise linearization, or a different solver would need to be applied. Regardless, the change in the objective function might increase the necessary computing time to solve the model.

The operational costs comprise the costs for external utility supply and an optional penalty for the duration of the process. In this work, we penalize the duration of the process in the single objective function directly and perform a single-objective optimization. Alternatively, a bi-objective optimization could be performed, with the investment and utility costs as one objective function and the process duration as the other, as we have shown in (Hagedorn et al., 2023). Again, specific cost factors for each term ($cost^{HU}$, $cost^{CU}$ and $cost^{time}$) are predefined as parameters.

$$\boldsymbol{cost^{operation,\ total}} = \sum_{c \in C} cost_c^{Ut} \cdot \boldsymbol{Q_c^{Ut}} + \sum_{h \in H} cost_h^{Ut} \cdot \boldsymbol{Q_h^{Ut}} + cost^{time} \cdot \boldsymbol{dur} \tag{9}$$

To derive the optimal design and operation of a heat integrated batch process, the temporal temperature profiles, and the spatial temperature profiles in the heat exchangers must be assessed. We model the temporal and spatial temperature profiles by ordinary differential equations as derived in section 2.3.

External heat exchangers:

The basic differential equation (Eq. (4)) for the external heat exchangers is derived in the previous section 2.3.

$$\dot{m}_m^{HI,cold} \cdot \boldsymbol{c_{p,m}^{HI,cold}} \cdot \frac{\boldsymbol{dT_m^{HI,cold}}\left(\boldsymbol{a_m^{HI}}, \boldsymbol{t}\right)}{\boldsymbol{da_m^{HI}}} = \boldsymbol{x_m^{HI}}\left(\boldsymbol{a_m^{HI}}\right) \cdot \boldsymbol{x_m^{t,HI}}(\boldsymbol{t}) \cdot \boldsymbol{k} \cdot \left(\boldsymbol{T_m^{HI,cold}}\left(\boldsymbol{a_m^{HI}}, \boldsymbol{t}\right) - \boldsymbol{T_m^{HI,hot}}\left(\boldsymbol{a_m^{HI}}, \boldsymbol{t}\right)\right) \quad \forall\ m \in M \tag{10}$$

Analogously to Equation (10), the ODE for the hot side of an external heat exchanger is:

$$\dot{m}_m^{HI,hot} \cdot c_{p,m}^{HI,hot} \cdot \frac{d\boldsymbol{T_m^{HI,hot}}\left(a_m^{HI}, t\right)}{da_m^{HI}} = \boldsymbol{x_m^{HI}}\left(a_m^{HI}\right) \cdot \boldsymbol{x_m^{t,HI}}(t) \cdot k \cdot \left(\boldsymbol{T_m^{HI,cold}}\left(a_m^{HI}, t\right) - \boldsymbol{T_m^{HI,hot}}\left(a_m^{HI}, t\right)\right) \quad \forall\ m \in M \tag{11}$$

Heat exchangers in the vessels:

Furthermore, the ODE for the heat exchangers in the hot vessels is:

$$\dot{m}_h^{HTM} \cdot c_{p,h}^{HTM} \cdot \frac{d\boldsymbol{T_h^{HTM}}\left(a_h^V, t\right)}{da_h^V} = \boldsymbol{x_h^V}\left(a_h^V\right) \cdot \boldsymbol{x_h^{t,Ut}}(t) \cdot k \cdot \left(\boldsymbol{T_h^V}(t) - \boldsymbol{T_h^{HTM}}\left(a_h^V, t\right)\right) \quad \forall\ h \in H \tag{12}$$

with the mass flow rate $\dot{m}_h^{HTM}$, the specific heat capacity $c_{p,h}^{HTM}$ and the local current temperature $T_h^{HTM,V}$ of the heat transfer medium, and the current vessel temperature $T_h^V(t)$. As derived in section 2.3, the binaries $x_c^V(a_c^V)$ and $x_c^{t,Ut}(t)$ are used to activate the differential equation only for the range of validity, i.e., the binaries deactivate the differential equation for bigger heat exchanger surface areas and longer heat supply durations than the optimum.

For the cold vessels, the ODE is defined accordingly as:

$$\dot{m}_c^{HTM} \cdot c_{p,c}^{HTM} \cdot \frac{d\boldsymbol{T_c^{HTM}}\left(a_c^V, t\right)}{da_c^V} = \boldsymbol{x_c^V}\left(a_c^V\right) \cdot \boldsymbol{x_c^{t,Ut}}(t) \cdot k \cdot \left(\boldsymbol{T_c^V}(t) - \boldsymbol{T_c^{HTM}}\left(a_c^V, t\right)\right) \quad \forall\ c \in C \tag{13}$$

Note that in comparison to the external heat exchangers, in the ODEs for the heat exchangers in the vessels, the temperatures at one side of the heat exchanger, i.e., the vessel temperatures $\boldsymbol{T_h^V}(t)$ and $\boldsymbol{T_c^V}(t)$, only depend on the time and not on the heat exchanger surface area, as we assume perfect mixture in the vessels.

Furthermore, the energy balance for the cold and the hot vessels must be fulfilled which are modeled as temporal differential equations for the cold vessels:

$$m_c^V \cdot c_{p,c}^V \cdot \frac{d\boldsymbol{T_c^V}(t)}{dt} = \dot{m}_c^{HTM} \cdot c_{p,c}^{HTM} \cdot \left(\boldsymbol{T_c^{HTM}}\left(a_c^V = 0, t\right) - \boldsymbol{T_c^{HTM}}\left(a_c^V = A_c^{V,\max}, t\right)\right) \quad \forall c \in C \tag{14}$$

and for the hot vessels:

$$m_h^V \cdot c_{p,h}^V \cdot \frac{d\boldsymbol{T_h^V}(t)}{dt} = \dot{m}_h^{HTM} \cdot c_{p,h}^{HTM} \cdot \left(\boldsymbol{T_h^{HTM}}\left(a_h^V = 0, t\right) - \boldsymbol{T_h^{HTM}}\left(a_h^V = A_h^{V,\max}, t\right)\right) \quad \forall h \in H \tag{15}$$

with m_c^V and m_h^V being the mass of the vessel fluids, and $c_{p,c}^V$ and $c_{p,h}^V$ the specific heat capacity of the vessel fluids.

Utility supply:

With the assumption of sequential operation, after the heat integration, utility supply will take place if needed. For the utility supply, differential equations analogously to the heat integration can be formulated:

$$\dot{m}_c^{HTM}\cdot c_{p,c}^{HTM}\cdot\frac{d\boldsymbol{T}_c^{Ut}\left(a_c^{Ut},t\right)}{da_c^{Ut}} = \boldsymbol{x}_c^{Ut}\left(a_c^{Ut}\right)\cdot\left(1-\boldsymbol{x}_{m_c}^{t,HI}(t)\right)\cdot\boldsymbol{x}_c^{t,Ut}(t)\cdot k\cdot\left(\boldsymbol{T}_c^{Ut}\left(a_c^{Ut},t\right)-\boldsymbol{T}_c^{Ut,sup}\left(a_c^{Ut},t\right)\right) \quad \forall\, c\in C \tag{16}$$

with $\boldsymbol{T}_c^{Ut}(a_c^{Ut},t)$ being the temperature of the heat transfer medium in the heat exchanger for utilities, and $\boldsymbol{T}_c^{Ut,sup}(a_c^{Ut},t)$ being the temperature of the external utility. Again, binaries $x_c^{Ut}(a_c^V)$ and $x_c^{t,Ut}(t)$ are used to activate the differential equation only for the range of validity.

Furthermore, as utility supply is only allowed after heat integration is finished, the corresponding binary $\boldsymbol{x}_{m_c}^{t,HI}$ is included in the formulation to switch utility supply off, during heat integration. Here, the index m_c corresponds to the predefined one-by-one match for the cold vessel.

On the utility supply side, the ODE is:

$$\dot{m}_c^{Ut}\cdot c_{p,c}^{Ut}\cdot\frac{d\boldsymbol{T}_c^{Ut,sup}\left(a_c^{Ut},t\right)}{da_c^{Ut}} = \boldsymbol{x}_c^{Ut}\left(a_c^{Ut}\right)\cdot\left(1-\boldsymbol{x}_{m_c}^{t,HI}(t)\right)\cdot\boldsymbol{x}_c^{t,Ut}(t)\cdot k\cdot\left(\boldsymbol{T}_c^{Ut}\left(a_c^{Ut},t\right)-\boldsymbol{T}_c^{Ut,sup}\left(a_c^{Ut},t\right)\right) \quad \forall c\in C \tag{17}$$

with $\dot{m}_c^{Ut}$ being the mass flow rate and $c_{p,c}^{Ut}$ being the heat capacity of the external utility.

For the utility supply for hot vessels, the constraints are defined accordingly as

$$\dot{m}_h^{HTM}\cdot c_{p,h}^{HTM}\cdot\frac{d\boldsymbol{T}_h^{Ut}\left(a_h^{Ut},t\right)}{da_h^{Ut}} = \boldsymbol{x}_h^{Ut}\left(a_h^{Ut}\right)\cdot\left(1-\boldsymbol{x}_{m_h}^{t,HI}(t)\right)\cdot\boldsymbol{x}_h^{t,Ut}(t)\cdot k\cdot\left(\boldsymbol{T}_h^{Ut,sup}\left(a_h^{Ut},t\right)-\boldsymbol{T}_h^{Ut}\left(a_h^{Ut},t\right)\right) \quad \forall\, h\in H \tag{18}$$

for the side of the heat transfer media, and for the utility side:

$$\dot{m}_h^{Ut}\cdot c_{p,h}^{Ut}\cdot\frac{d\boldsymbol{T}_h^{Ut,sup}\left(a_h^{Ut},t\right)}{da_h^{Ut}} = \boldsymbol{x}_h^{Ut}\left(a_h^{Ut}\right)\cdot\left(1-\boldsymbol{x}_{m_h}^{t,HI}(t)\right)\cdot\boldsymbol{x}_h^{t,Ut}(t)\cdot k\cdot\left(\boldsymbol{T}_h^{Ut,sup}\left(a_h^{Ut},t\right)-\boldsymbol{T}_h^{Ut}\left(a_h^{Ut},t\right)\right) \quad \forall\, h\in H \tag{19}$$

The overall utility demand for a hot vessel $\boldsymbol{Q}_h^{CU}$ and a cold vessel $\boldsymbol{Q}_c^{HU}$ is then the temporal integral over the heating power and cooling power supplied by the utilities:

$$\boldsymbol{Q}_h^{Ut} = \int_{t\in[dur^{HI}:dur]}\dot{m}_h^{Ut}\cdot c_{p,h}^{Ut}\cdot\left(\boldsymbol{T}_h^{Ut,sup}\left(a_h^{Ut}=0,t\right)-\boldsymbol{T}_h^{Ut,sup}\left(a_h^{Ut}=a^{\max},t\right)\right)dt \quad \forall\, h\in H \tag{20}$$

$$\boldsymbol{Q}_c^{Ut} = \int_{t\in[dur^{HI}:dur]}\dot{m}_c^{Ut}\cdot c_{p,c}^{Ut}\cdot\left(\boldsymbol{T}_{c^{Ut,sup}}\left(a_c^{Ut}=0,t\right)-\boldsymbol{T}_c^{Ut,sup}\left(a_c^{Ut}=a^{\max},t\right)\right)dt\forall c\in C \tag{21}$$

Finally, the binaries used to activate and deactivate the differential equations, indicate the optimal heat exchanger areas and the duration of the heat integration process and of the utility supply.

$$\boldsymbol{A}_m^{HI}\geq\boldsymbol{x}_m^{HI}\left(a_m^{HI}\right)\cdot a_m^{HI} \quad \forall m\in M \tag{22a}$$

$$\boldsymbol{A}_h^{Ut}\geq\boldsymbol{x}_h^{Ut}\left(a_h^{Ut}\right)\cdot a_h^{Ut} \quad \forall h\in H \tag{22b}$$

$$\boldsymbol{A}_c^{Ut}\geq\boldsymbol{x}_c^{Ut}\left(a_c^{Ut}\right)\cdot a_c^{Ut} \quad \forall c\in C \tag{22c}$$

$$\boldsymbol{A}_h^{V}\geq\boldsymbol{x}_h^{V}\left(a_h^{V}\right)\cdot a_h^{V} \quad \forall h\in H \tag{22d}$$

$$\boldsymbol{A}_c^{V}\geq\boldsymbol{x}_c^{V}\left(a_c^{V}\right)\cdot a_c^{V} \quad \forall c\in C \tag{22e}$$

$$\boldsymbol{dur}_m^{HI}\geq\boldsymbol{x}_m^{t,HI}(t)\cdot t \quad \forall m\in M \tag{22f}$$

$$\boldsymbol{dur}_h^{Ut}\geq\boldsymbol{x}_h^{t,Ut}(t)\cdot t \quad \forall h\in H \tag{22g}$$

$$\boldsymbol{dur}_c^{Ut}\geq\boldsymbol{x}_c^{t,Ut}(t)\cdot t \quad \forall c\in C \tag{22h}$$

$$\boldsymbol{dur}\geq\boldsymbol{dur}_c^{Ut} \quad \forall c\in C \tag{22i}$$

$$\boldsymbol{dur}\geq\boldsymbol{dur}_h^{Ut} \quad \forall h\in H \tag{22j}$$

2.5. Discretization by orthogonal collocation on finite elements

To solve the dynamic Dyn2Heat optimization model, we apply a direct transcription method to simultaneously discretize the whole model. We implement the direct transcription method using pyomo.dae (Nicholson et al., 2018). We choose the direct transcription method as a solution approach, as it transforms the dynamic optimization model into a purely algebraic problem, which can then be solved by off-the-shelf solvers for algebraic optimization problems. Furthermore, direct transcription allows for integer variables in the optimization problem, as they are present in the Dyn2Heat model. As a discretization scheme, we use orthogonal collocation, which is already implemented in pyomo.dae (Nicholson et al., 2018).

For the transcription, the continuous domains a_m^{HI}, a_h^V, a_c^V, a_h^{Ut}, a_c^{Ut} and t are discretized into finite elements $i\in I$. The state variables of the differential equations, i.e., the temperatures in the Dyn2Heat model, are then approximated by piecewise polynomials. In every finite element i, a polynomial of degree K is defined for each state variable. In a power series representation such a polynomial for the exemplary temperature $T(t)$ in finite element i is given as

$$T^K(t)=p_{i,0}+\ p_{i,1}\cdot t+p_{i,2}\cdot t^2+\ldots\ +p_{i,K}\cdot t^K;\ t\in[t_{i-1}:t_i] \tag{23}$$

Each finite element includes K collocation points that serve, together with the boundaries of the finite elements, as the interpolation points of the polynomial (Fig. 3). At these interpolation points the polynomial must be equal to the solution to the differential equation. Thus, to derive appropriate polynomial coefficients $p_{i,(0,\ldots,K)}$, the derivative of Eq. (23) is substituted into the original differential equation. The resulting algebraic equation is called collocation equation and is enforced at the interpolation points. Based on these interpolation points, the piece-wise polynomials approximate the original differential equation. Instead of the power series representation, we use Lagrange polynomials as a polynomial representation. The respective collocation equation is given in Appendix C. The collocation points are positioned relative to the finite element boundaries following the Gauss-Radau scheme.

Integrals in the Dyn2Heat problem are approximated by the trapezoid rule. The resulting discretized problem is a mixed-integer linear (MILP) optimization problem that can be solved by off-the-shelf solvers. For more information on the direct transcription method, the reader is referred to (Biegler, 2010) and for information on the implementation in pyomo.dae, the reader is referred to (Nicholson et al., 2018).

In the discretized Dyn2Heat problem, the binary variables $\boldsymbol{x}^{t,Ut}(t)$, $\boldsymbol{x}_m^{t,HI}(t)$, $\boldsymbol{x}_m^{HI}(a_m^{HI})$, $\boldsymbol{x}_h^{V}(a_h^{V})$, $\boldsymbol{x}_c^{V}(a_c^{V})$, $\boldsymbol{x}_h^{Ut}(a_h^{Ut})$ and $\boldsymbol{x}_c^{Ut}(a_c^{Ut})$ indicate which finite elements are used for heat integration, i.e., in which finite elements the differential equations are active. The duration and the heat exchanger sizes can only take the discrete values of the discretized continuous domains, i.e., the binaries can only switch from 1 to 0 at the edges of the finite elements. Accordingly, the solution to the discretized

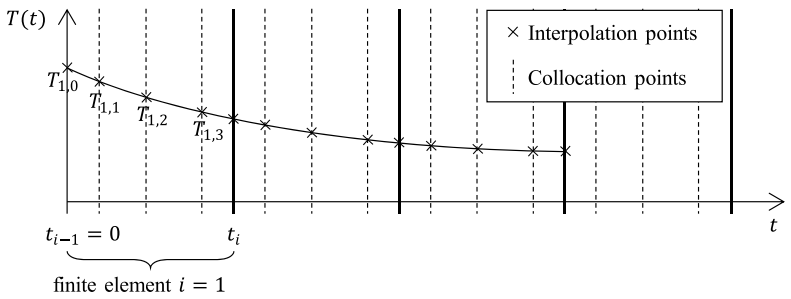


Fig. 3. Profile of the exemplary temperature $T(t)$ over time t. Applying orthogonal collocation, the original state profile, i.e., the solution to the differential equation, is approximated by piecewise polynomials. For the piecewise polynomials, the continuous time domain is separated into finite elements $i \in I$ (solid lines). In each finite element, a polynomial is defined. The finite elements each contain K collocation points (dashed lines). Together with the boundaries of the finite elements, the collocation points serve as interpolation points (marked as crosses) for the piecewise polynomial with degree K (here $K = 3$). The figure is oriented to (Biegler, 2010).

problem can be found at the last collocation point of each finite element. Thus, the accuracy of the solution increases with decreasing step size of the discretization. On the other hand, a fine resolution of the finite elements leads to bigger problems and thus to longer computing times. As a result, there is a trade-off between model accuracy and problem size that can be influenced by the selection of the finite elements for discretization.

2.6. Iterative refinement method

To address the trade-off between model accuracy and problem size, we propose an iterative refinement method for the discretization of the continuous domains. The refinement method iteratively solves the discretized model with increasing resolution of finite elements in the surrounding of the problem solution, while restricting the feasible solution space successively (Fig. 4). Hence, the approach of the refinement method leads to a local refinement of the discretized domains only in the surrounding of the solution, while the overall resolution of the discretized domains is kept coarse. By this, the refinement method solves the Dyn2Heat model efficiently. In an initial run, the optimization problem is solved with a user-defined coarse resolution, i.e., only few finite elements, in all discretized domains. Afterwards, the feasible solution space for the next run is constrained, by fixing the binaries $(\boldsymbol{x}^{\boldsymbol{t,Ut}}(t), \boldsymbol{x}_{\boldsymbol{m}}^{\boldsymbol{t,HI}}(t), \boldsymbol{x}_{\boldsymbol{m}}^{\boldsymbol{HI}}(a_m^{HI}), \boldsymbol{x}_{\boldsymbol{h}}^{\boldsymbol{V}}(a_h^V), \boldsymbol{x}_{\boldsymbol{c}}^{\boldsymbol{V}}(a_c^V), \boldsymbol{x}_{\boldsymbol{h}}^{\boldsymbol{Ut}}(a_h^{Ut})$ and $\boldsymbol{x}_{\boldsymbol{c}}^{\boldsymbol{Ut}}(a_c^{Ut}))$ around the solution found. In detail, the binaries for index values smaller than the solution are set to be 1, while the binaries for index values bigger than the solution are set to be 0.

However, a small valid interval with unfixed binaries in the direct surrounding of the optimum is kept as the feasible solution space for the next optimization. Within this valid interval, the number of finite elements is increased compared to the previous run, resulting in a finer resolution of the discretized domain in the surrounding of the optimum. In the next optimization, the problem is resolved with the restricted solution space and the finer resolution in the valid interval. The finer resolution leads to a higher accuracy in the approximation of the differential equations and to more discrete possible values for the heat exchanger areas and the process durations in the surrounding of the optimum. At the same time, the resolution outside of the valid interval is the same as in the previous run, to keep the number of finite elements low. The refinement step can be repeated iteratively until the desired resolution is reached in the surrounding of the optimum.

The size of the valid interval should be chosen carefully. A bigger interval leads to bigger problem size, while an interval that is chosen too small may exclude the real optimum. We recommend selecting the valid interval for the next run by the size of one finite element below the current optimum and to the edge of the next finite element above the current optimum (Fig. 4). We found that this heuristic worked well in a small study with varying size of valid intervals. For the time domain, two valid intervals are kept: one interval for the optimal duration of heat integration, and one for the optimal overall process duration. If the two intervals overlap, they are merged to one common valid interval.

All in all, the iterative refinement method can reduce the computational time while maintaining high accuracy, as the problem size is kept small for each iteration, although the resolution in the surrounding of the optimum is increased.

Note that in this work, the resolution of each run and the number of iterations are predefined as input parameters of the refinement algorithm. However, more sophisticated rules for the optimal refinement steps and the termination of the refinement method could be developed in future works.

3. Simplified Case Study: Comparison to an Algebraic Optimization Model

3.1. Nonlinear Algebraic Benchmark Models

In the following, we evaluate the Dyn2Heat model formulation by comparing the performance of the Dyn2Heat model to an algebraic benchmark model based on the LMTD function. We define a case study, adapted from a milk pasteurization process. A more detailed description of the case study is given in section 3.2.

The goal of this first case study is to validate the model by comparing the solution to the solution of the algebraic benchmark model. Furthermore, the computational performance of the Dyn2Heat model is evaluated in comparison to the algebraic benchmark. In order to be able to solve the algebraic benchmark model, we use a simplified system setup, where no heat transfer medium is used, but the vessel fluid, i.e., the milk, is transferred through the optional external heat exchanger directly (Fig. 5). Furthermore, we only model the heat integration in detail, and simplify the utility transfer by only modeling the remaining heating and cooling demand as energy demands after heat integration is finished.

Adaption of the Dyn2Heat model to the simplified case study:

To adapt the Dyn2Heat model to this setup, equations (12) and (13) are neglected. Instead, the vessel temperatures are connected to the inlet temperatures of the external heat exchanger directly.

Furthermore, equations (16) - (21) for the utility supply are neglected. Instead, the following energy balances for the vessels are included to derive the utility demand:

$$\boldsymbol{Q}_{\boldsymbol{c}}^{\boldsymbol{Ut}} = m_c^V \cdot c_{\mathrm{p},c}^V \cdot \left(T_c^{V,target} - \boldsymbol{T}_{\boldsymbol{c}}^{\boldsymbol{V}}\left(t = dur^{HI}\right)\right) \tag{24}$$

$$\boldsymbol{Q}_{\boldsymbol{h}}^{\boldsymbol{Ut}} = m_h^V \cdot c_{\mathrm{p},h}^V \cdot \left(\boldsymbol{T}_{\boldsymbol{h}}^{\boldsymbol{V}}\left(t = dur^{HI}\right) - T_h^{V,target}\right) \tag{25}$$

Although the setup is rather simplified, it still covers the main elements of the Dyn2Heat model. Namely, the external heat exchanger is described by the ODEs (Eq. (10) and (11)) and the dynamics in the

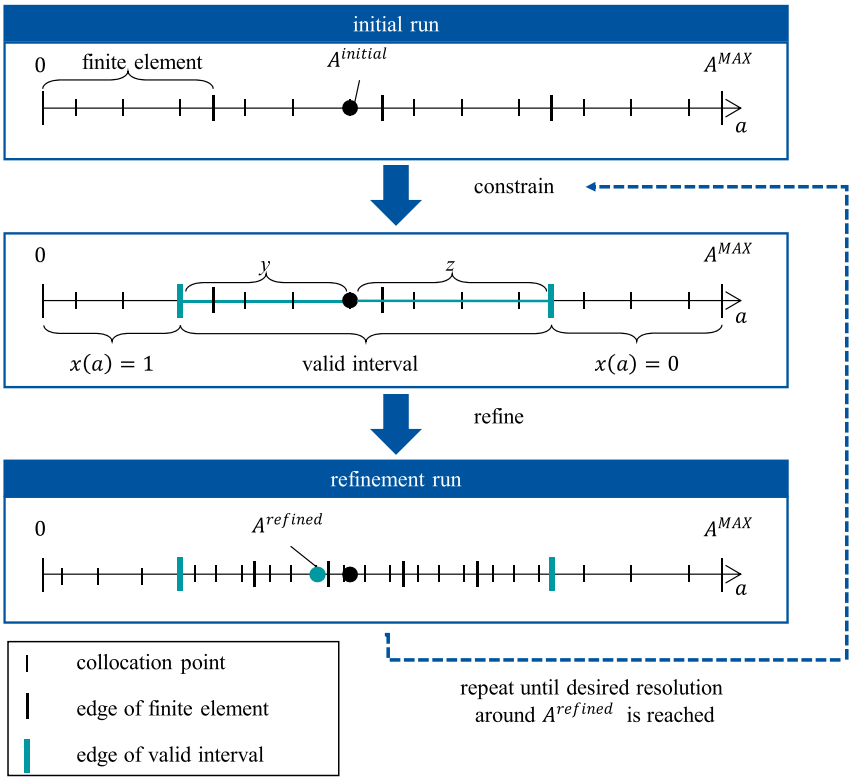


Fig. 4. Scheme of the refinement algorithm for one exemplary heat exchanger area A. In the initial run, the whole interval $[0; A^{MAX}]$ is a feasible solution space for the optimal heat exchanger area A. After the first run, the feasible solution space is restricted to the surrounding of the previously found solution $A^{initial}$, by fixing the values of the corresponding binaries $x(a)$ apart from this new valid interval. We recommend selecting the valid interval for the next run by the size of one finite element below the current optimum (y) and to the edge of the next finite element above the current optimum (z). In the next run, the discretization is refined within the valid interval, leading to a higher accuracy of the discretized model.

vessels are still described by the ODEs (Eq. (14) and (15)). As an objective function, the overall costs comprising operational costs for utility supply, investment costs for the optional external heat exchanger and penalty costs for the duration of the heat integration, are minimized. To solve the Dyn2Heat model for the simplified case study, we apply the direct transcription method based on orthogonal collocation with the iterative refinement method as proposed above.

The algebraic benchmark model:

In the following, we introduce the central model equations of the algebraic benchmark model. The detailed model equations are given in Appendix CAppendix . The benchmark model uses the mean temperature difference over the heat exchanger area and over the process duration instead of the dynamic temperature profiles to model the heat exchange. Thus, the benchmark model is a fully algebraic model and does not include any differential equations. The mean temperature difference is a double logarithmic expression $\boldsymbol{LMTD^{total}}$ (Eq. (26)). The derivation of $\boldsymbol{LMTD^{total}}$ follows (Glück, 2017). $\boldsymbol{LMTD^{total}}$ comprises the local logarithmic mean temperature difference over time ($\boldsymbol{LMTD^{time}}$) at the hot side of the heat exchanger ($a^{HI} = 0$) (Eq.(27)), and the current logarithmic mean temperature difference over the heat exchanger area ($\boldsymbol{LMTD^{area}}$) at the beginning of the heat integration ($t = 0$) (Eq.(28)). The product of the two mean temperature differences is normalized by the absolute temperature difference at the hot side of the heat exchanger at the beginning of the heat integration ($T^{HI,hot}(0,\ 0) - \boldsymbol{T^{HI,cold}}(0,\ 0)$).

$$\boldsymbol{LMTD^{total}} = \frac{1}{T^{HI,hot}(0,\ 0) - \boldsymbol{T^{HI,cold}}(0,\ 0)} \cdot \boldsymbol{LMTD^{area,t0}} \cdot \boldsymbol{LMTD^{time}} \tag{26}$$

with

$$\boldsymbol{LMTD^{time}} = \frac{\left(T^{HI,hot}(0,0) - \boldsymbol{T^{HI,cold}}(0,0)\right) - \left(\boldsymbol{T^{HI,hot}}(0, dur^{HI}) - \boldsymbol{T^{HI,cold}}(0, dur^{HI})\right)}{ln\left(T^{HI,hot}(0,0) - \boldsymbol{T^{HI,cold}}(0,0)\right) - ln\left(\boldsymbol{T^{HI,hot}}(0, dur^{HI}) - \boldsymbol{T^{HI,cold}}(0, dur^{HI})\right)} \tag{27}$$

and

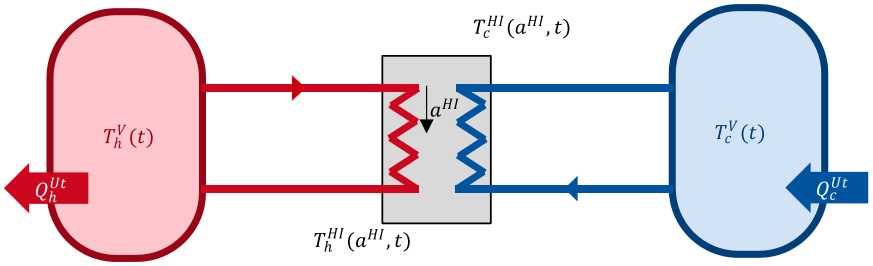


Fig. 5. Setup of the simplified case study without heat exchangers in the vessels and without explicit modelling of utility supply.

Table 1
Comparison of the results for the simplified case study.

	Dyn2Heat	LMTD	Chen
Total costs per batch	$7,55\frac{€}{batch}$	$7,30\frac{€}{batch}$	$7,62\frac{€}{batch}$
Optimal HEX area	$12,04\ m^2$	$13,87\ m^2$	$11,94\ m^2$
Optimal HI time	147 *sec*	159 *sec*	126 *sec*
Computing time (total)	134, 18 *sec* (98 sec for optimization)	43 200 *sec* (abort by max. computing time at rel. gap 4, 9 %)	43 200 *sec* (abort by max. computing time at rel. gap 5 %)

$$\boldsymbol{LMTD}^{\boldsymbol{area},t0} = \frac{\left(T^{HI,hot}(0,0) - \boldsymbol{T}^{\boldsymbol{HI,cold}}(0,0)\right) - \left(\boldsymbol{T}^{\boldsymbol{HI,hot}}\left(A^{HI}_{h,c},0\right) - T^{HI,cold}\left(A^{HI}_{h,c},0\right)\right)}{ln\left(T^{HI,hot}(0,0) - \boldsymbol{T}^{\boldsymbol{HI,cold}}(0,0)\right) - ln\left(\boldsymbol{T}^{\boldsymbol{HI,hot}}\left(A^{HI}_{h,c},0\right) - T^{HI,cold}\left(A^{HI}_{h,c},0\right)\right)} \tag{28}$$

In the algebraic benchmark model, the $\boldsymbol{LMTD}^{\boldsymbol{total}}$ models the temperature profile, i.e. equations (26) - (28) replace the differential equation for the external heat exchanger (Eq.s (10) and (11)).

With the $\boldsymbol{LMTD}^{\boldsymbol{total}}$, the integrated heat is:

$$\boldsymbol{Q}^{\boldsymbol{HI}} = k \cdot \boldsymbol{A}^{\boldsymbol{HI}} \cdot \boldsymbol{LMTD}^{\boldsymbol{total}} \cdot \boldsymbol{dur}^{\boldsymbol{HI}} \tag{29}$$

and the optimal heat exchanger surface area can be derived from

$$k \cdot \boldsymbol{LMTD}^{\boldsymbol{area},t0} \cdot \boldsymbol{A}^{\boldsymbol{HI}} = \dot{m}_c \cdot \boldsymbol{c}_{p,c} \cdot \left(\boldsymbol{T}^{\boldsymbol{HI,cold}}(0,0) - T^{HI,cold}\left(A^{HI},0\right)\right) \tag{30}$$

$$k \cdot \boldsymbol{LMTD}^{\boldsymbol{area},t0} \cdot \boldsymbol{A}^{\boldsymbol{HI}} = \dot{m}_h \cdot c_{p,h} \cdot \left(\boldsymbol{T}^{\boldsymbol{HI,hot}}\left(A^{HI},0\right) - T^{HI,hot}(0,0)\right) \tag{31}$$

$$k \cdot \boldsymbol{LMTD}^{\boldsymbol{area},\ t^{HI}} \cdot \boldsymbol{A}^{\boldsymbol{HI}} = \dot{m}_c \cdot c_{p,c} \cdot \left(\boldsymbol{T}^{\boldsymbol{HI,cold}}\left(0, dur^{HI}\right) - \boldsymbol{T}^{\boldsymbol{HI,cold}}\left(A^{HI}, dur^{HI}\right)\right) \tag{32}$$

$$k \cdot \boldsymbol{LMTD}^{\boldsymbol{area},\ t^{HI}} \cdot \boldsymbol{A}^{\boldsymbol{HI}} = \dot{m}_h \cdot c_{p,h} \cdot \left(\boldsymbol{T}^{\boldsymbol{HI,hot}}\left(A^{HI}, dur^{HI}\right) - \boldsymbol{T}^{\boldsymbol{HI,hot}}\left(0, dur^{HI}\right)\right) \tag{33}$$

Instead of using the LMTD function, most existing models for HEND use an approximation or a robust reformulation. Thus, in addition to the original LMTD function, we use the Chen approximation (Chen, 1987) as another benchmark formulation. The Chen approximation approximates the LMTD for two temperature differences ΔT^A and ΔT^B as:

$$LMTD = \frac{\Delta T^A - \Delta T^B}{\ln\left(\frac{\Delta T^A}{\Delta T^B}\right)} \approx \left(\Delta T^A \cdot \Delta T^B \cdot \left(\frac{\Delta T^A + \Delta T^B}{2}\right)\right)^{\frac{1}{3}} \tag{34}$$

The Chen approximation can be implemented analogously to the LMTD in Equations (26) - (28) and replace the logarithmic mean temperature differences in the model.

3.2. Definition of the Simplified Case Study

In the following, we describe the simplified case study used to compare the computational efficiency of the dynamic Dyn2Heat model with the algebraic LMTD model. The case study is adapted from the milk pasteurization process, described in (Fellows, 2017).

For pasteurization, milk is first heated up to a temperature of 345.15 *K* and afterwards cooled down again to a final temperature of 277.65 *K*. For the case study, we assume batch operation, i.e., the milk is heated and cooled in vessels. We assume two vessels working in parallel, each containing 1000 *kg* of milk. The two vessels work time-shifted to each other, such that the cooling process in one vessel takes place at the same time as the heating process in the other vessel. By this time-shift, the surplus heat of the cooling process can directly be used in the heating process. Further input parameters are oriented to (Fellows, 2017) or set as assumptions by the authors. A detailed list of all input parameters is given in Appendix E.

For the orthogonal collocation, we use three collocation points per finite element, i.e., a polynomial degree of 3. For the refinement method, we use 5 iterations with the following step sizes in each iteration: for the time t in *sec*: $(200; 100; 50; 30; 10)$ and for the area a^{HI} in m^2: $(20; 10; 5; 3; 1)$. The upper bound for the area is set to 100 m^2 and the upper bound for the duration is set to 1000 *sec*. The resulting boundaries of the finite elements for the first run and the last run are given in Appendix E.

We implement the model with pyomo.dae (Nicholson et al., 2018) in python 3.7. Pyomo.dae is also used for the transformation by orthogonal collocation. We solve the discretized model with the MILP solver Gurobi in version 10.0.1 (Gurobi Optimization L.L.C.). The algebraic models are implemented in python 3.7 as well, and solved with the global MINLP solver Baron, version 22.11.3 (Sahinidis, 2024). All optimizations for the simplified case study are performed using 8 threads of an Intel Xeon at 3.2 GHz.

3.3. Results of the Simplified Case Study

We optimize the Dyn2Heat model for the introduced case study and compare the results to the algebraic model formulation. We solve the Dyn2Heat model in each iteration to a relative optimality gap of $1E-8$. For the algebraic models, i.e., the model based on the LMTD-function and the model based on the Chen approximation, we define a relative gap of $1E-4$ and a maximal computing time of 43 200 ***sec***, i.e., 12*hours*, as termination criteria. In the following, we compare the results of the different models. Table 1 gives an overview of the performance of the models.

For the considered case study, the solutions obtained differ only slightly between the different models. The comparison shows that all models, the Dyn2Heat model and the algebraic models, can describe the system accurately and find a feasible solution of good quality within reasonable computing time.

Fig. 6 shows different parts of the total costs for the Dyn2Heat model, the LMTD model and the Chen model. A big share ($4.18\ €/batch$) is caused by unavoidable utility use: the final temperature of the cooling process is lower than the final temperature of the heating process. Thus, the two vessels can physically not be fully supplied by heat integration, but utility supply is needed to provide the rest of the heating and cooling demand. For the remainder of the total cost, we see that the main difference results from different utility costs. The slight differences probably result from inaccuracies in the approximation of the temperature profiles in all models and from the assumptions made. In our comparison we found that the difference between the resulting temperature profiles were small. One possible reason for the inaccuracies in the Dyn2Heat model is the discretization of the spatial and temporal domain and the approximation of the temperature profiles by polynomials. However, the Dyn2Heat solution is within the range of the solutions of the LMTD model and the Chen model. In fact, we see that for the Dyn2Heat model, the values of both optimization variables, the heat exchanger area a^{HI} and the duration of heat integration *dur*, lie between the values of both algebraic models. Thus, we conclude that the Dyn2Heat model is sufficiently accurate for the considered case study and can design heat exchanger networks for dynamic batch processes with a good solution quality.

Fig. 7 shows the progression of the upper and lower bounds for the

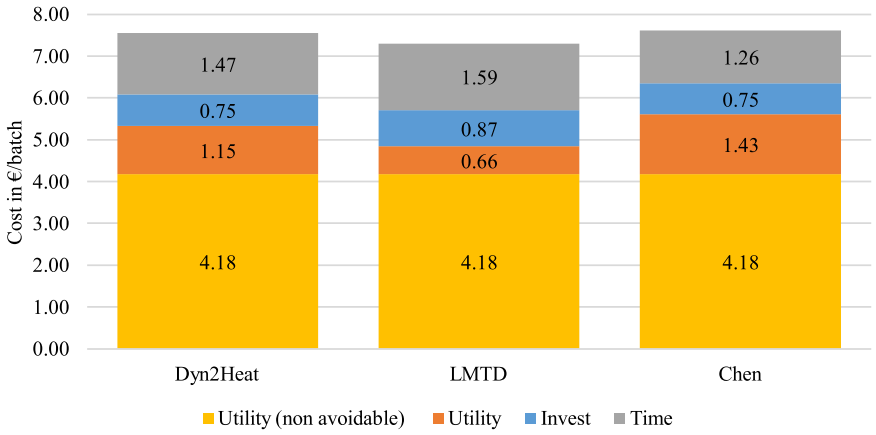


Fig. 6. Composition of the total costs per batch for the different models. The total costs comprise utility costs of which a part is unavoidable, investment costs for the external heat exchanger related to one batch run, and the time penalty.

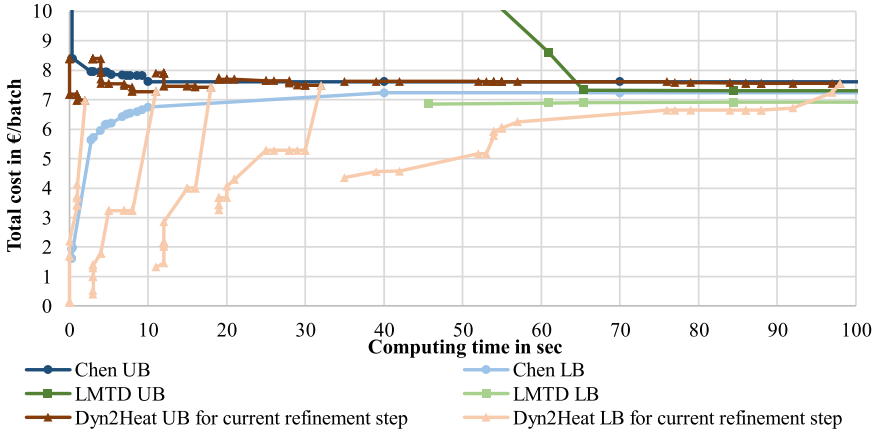


Fig. 7. Upper bounds (UB) and lower bounds (LB) plotted against the computing time for the different optimization models. For the Dyn2Heat model, the upper and lower bound for each individual refinement step are shown one after the other.

different models. For better readability, the axis for the total costs was cut at 10 $€/batch$. For the Dyn2Heat model, the upper and lower bound for each individual optimization run of the refinement method are shown one after the other.

With the chosen settings, the Dyn2Heat model terminates after 134.18 *sec* of which 98 *sec* are used for the cumulated optimization runs. Furthermore, the first iteration with a coarse resolution of 5 finite elements for both dimensions, area, and time, terminates after 1 *sec* and finds a good solution of 6.98 $€/batch$ already. However, the coarse resolution of 5 finite elements leads to only 5 discrete feasible values for the optimal time and area. In the regarded case study, the feasible values of the first iteration are by chance relatively close to the final solution ($a^{HI} = 12.98m^2$ and $dur = 128,99$ *sec*). Thus, a coarse resolution could potentially also lead to worse results. The overall computing time of the Dyn2Heat model strongly depends on the predefined refinement steps. Due to the refinement algorithm, the Dyn2Heat model can start with a coarse resolution and iteratively refine the resolution in the near surrounding of the optimum of the previous iteration. This way, each iteration is computationally efficient and can be solved in short computational time. The trade-off between computing time and accuracy can be adapted by choosing appropriate refinement steps.

In comparison, the algebraic benchmark model with the LMTD finds the first feasible solution of 12.38 $€/batch$ after 45.62 *sec*. The final upper bound of 7.30 $€/batch$ is reached after 84.51 *sec*. The algebraic benchmark model with the Chen approximation finds a feasible upper bound of 18.39 $€/batch$ much quicker after 1.6 *sec*. The final upper bound of 7.62 $€/batch$ is reached after 10.00 *sec*. However, the algebraic benchmark models cannot close the optimality gap of $1E-4$ within the allowed computing time of 43 200 *sec*, but a relative optimality gap of around 5 % remains for both.

In a second optimization, we test the models for a small change in the parameters of the case study, where we increase the mass flow rate through the heat exchanger slightly to $\dot{m}_h = 10\ kg/s$ (instead of $\dot{m}_h = 8\ kg/s$) for the hot side, and $\dot{m}_c = 12\ kg/s$ (instead of $\dot{m}_c = 10\ kg/s$) for the cold side. For this setup, we find that the LMTD model does not find any feasible solution within 43200 *sec*, while the Dyn2Heat model finds a solution of 7.41 $€/batch$ within 185.60 *sec* and the Chen model finds a solution of 7.46 $€/batch$ in 32.04 *sec*. However, the Chen model, again, cannot close the optimality gap within 43200 *sec*, but a gap of 5 % remains. In our work, we used Baron as a global solver for the mixed-integer nonlinear benchmark problems (Sahinidis, 2024). A dedicated solution algorithm for the benchmark problems could also improve the performance of the benchmark models. A promising solution algorithm for heat exchanger network design problems including the LMTD function was proposed by Mistry and Misener (Mistry and Misener, 2016). It would be beneficial to evaluate such solution algorithms for the benchmark models in future works. All in all, we conclude that the Dyn2Heat model can find good solutions to the dynamic heat integration problem within short computational time. The model can compete or even outperform the nonlinear algebraic benchmark models regarding the computational efficiency. The Dyn2Heat model has the further advantage that the trade-off between solution accuracy and model complexity can be adjusted due to the discretization. The small

parameter changes in the case study show that the Dyn2Heat model finds good solutions more reliably than the nonlinear LMTD formulation. Furthermore, by the direct transcription, the Dyn2Heat model reduces to an MILP problem, which is why we assume that the Dyn2Heat problem can also be reliably applied to larger problems. We test the Dyn2Heat model in a more complex case study in the next section.

4. Application to a More Complex Case Study

In a second case study, we apply the Dyn2Heat model to the non-simplified setup introduced in the model definition (Fig. 2). The non-simplified setup models the utility supply explicitly and uses a heat transfer medium. The case study considers two different operation modes which significantly increases the complexity of the case study in comparison to the simplified version. Furthermore, there are now five possible heat exchangers involved instead of one in the simplified version. We consider the same milk pasteurization process as in the simplified case study, oriented to (Fellows, 2017). Thus, the parameters are adopted from the simplified case study. Additional parameters for the complex case study are given in Appendix E.

We run the complex case study using 16 threads of an Intel Xeon Platinum at 2.1 GHz. The final solution leads to total costs of 14.63 $€/batch$. The total costs are composed of 3.10 $€/batch$ for investments (21% of total costs), 4.40 $€/batch$ for utility supply (30% of total costs) and 7.13 $€/batch$ as a time penalty (49% of total costs). The heat integration and utility supply are realized by heat exchangers of the sizes given in Table 2.

Fig. 8 shows the temperature progression of the fluid temperatures over time. Heat integration is used until $\Delta T^{min} = 5.87\ K$ is reached after $t^{HI} = 411.60\ sec$. Afterwards, utility supply takes place till the final target temperatures are reached at 1 427.00 sec.

What is striking is that neither the heat exchanger sizes, nor the process duration are at their variable bounds, i.e., we conclude that for the considered case study, there is a trade-off between investment costs, operational costs, and process duration and that the Dyn2Heat model can capture this trade-off.

In detail, we observe that the process duration is longer in comparison to the simplified case study without explicit modelling of the utility supply. The longer process duration has several reasons: In the complex case study the process duration includes the utility supply which takes additional time, whereas, in the simplified case study, the utility supply is only defined by the remaining heating and cooling demands and neglected for the process duration. To account for the inherent additional time, we reduced the time penalty for the second case study by a factor of two, which makes a short process duration economically less important. Furthermore, due to the usage of a heat transfer medium, the heat transfer is less efficient than in the simplified case study.

Regarding the heat exchanger sizes, we find that in the cold vessel, a larger heat exchanger is installed than in the hot vessel. We explain this result by the fact that in the considered case study, the heat transfer medium used in the cold vessel was assumed to have a higher heat capacity flow rate than the heat transfer medium in the hot vessel. Thus, a larger heat exchanger can be valuable to reach smaller temperature differences at the outlet. Fig. 8 shows the resulting smaller temperature difference between the heat transfer medium at the cold side $\boldsymbol{T_c^{HTM}}(A_c^V, t)$ and the cold vessel temperature $\boldsymbol{T_c^V}(t)$, and the heat transfer medium at the hot side $\boldsymbol{T_h^{HTM}}(A_h^V)$ and the hot vessel temperature $\boldsymbol{T_h^V}(t)$.

Furthermore, due to the bigger heat capacity flow rate of the heat transfer medium at the cold vessel side, the temperature difference between inlet and outlet at the external heat exchanger, i.e., $\boldsymbol{T_c^{HTM}}(0,t) - \boldsymbol{T_c^{HTM}}(A_c^V,t)$, is in any time point smaller than the temperature difference on the hot side, i.e., $\boldsymbol{T_h^{HTM}}(A_h^V,t) - \boldsymbol{T_h^{HTM}}(0,t)$. We find that the average temperature of both heat transfer media increases during heat integration, which supports the cooling of the hot vessel at the beginning of the process. Note that in our case study, we did not fix the starting conditions for the heat transfer media, which gives the degree of freedom to choose the optimal start temperatures. However, if needed, it would be possible to fix the start temperature of the heat transfer media in advance.

For the utility, the cold vessel needs a significantly smaller heat exchanger and still reaches its final temperature more quickly than the hot vessel. One reason is again the higher heat capacity flow rate of the heat transfer medium in the cold vessel. Furthermore, the temperature difference between the hot utility and the cold vessel ($\boldsymbol{T_c^{Ut,sup}}(A_c^{Ut},t) - \boldsymbol{T_c^V}(t)$) is bigger than the temperature difference between the cold utility and the hot vessel ($\boldsymbol{T_h^V}(t) - \boldsymbol{T_h^{Ut,sup}}(0,t)$). Thus, more heat can be transferred to the cold vessel in shorter time than transferred from the hot vessel to the cold utility, although the heat exchanger is of smaller size.

Regarding the computational efficiency, the refinement algorithm for the complex case study terminates after 16.22 h (16.21 h for optimization). Fig. 9 shows the progression of the upper- and lower- bound in each refinement step.

In comparison to the simplified case study, the bigger case study needs remarkably longer computing time to terminate, although being performed with more computing resources. Still, 16.22 h is an acceptable computing time for design problems. In the first iteration, a good solution (deviation of 8% in objective function value compared to final solution) is found after 22.17 min. Furthermore, a good feasible solution (upper bound) is quickly found in each refinement run in comparison to the convergence of the lower bound. Therefore, with a strict time limit, Dyn2Heat could also serve as an approximation method to identify fair solutions with low computational effort.

We also adapt the nonlinear algebraic benchmark model based on the Chen approximation to the second case study and test it with the same computing resources as the Dyn2Heat model. As a solver, again Baron is used (Sahinidis, 2024). For the benchmark model, no feasible solution was found within the allowed computing time of 24 h. Again, sophisticated solution algorithms could improve the performance of the benchmark model. Nevertheless, the big difference in computational performance underlines the superiority of the Dyn2Heat model.

We conclude that the Dyn2Heat model leads to a reasonable solution for the complex case study. In comparison, the algebraic benchmark models are already hard to solve for the simplified case study and could not find a feasible solution for the complex case study within the set time limit. The solution of the Dyn2Heat model meets the trade-off between investment and utility costs and the process duration. To the best of our knowledge, no existing model could solve the regarded problem in the same accuracy as the Dyn2Heat model. The results of the complex case study underline the value of the Dyn2Heat model as a mathematical optimization model for the design of heat exchanger networks for batch processes, even for complex setups.

Table 2
Overview of the optimal heat exchanger sizes for the complex case study.

Description of the variable	Symbol	Value
Heat exchanger surface area for heat integration	A_m^{HI}	10.30 m^2
Heat exchanger surface area in hot vessel	A_h^V	11.20 m^2
Heat exchanger surface area in cold vessel	A_c^V	20.11 m^2
Heat exchanger surface area for cold utility supply	A_h^{Ut}	5.94 m^2
Heat exchanger surface area for hot utility supply	A_c^{Ut}	2.00 m^2

5. Conclusions

In this work, we introduce the Dyn2Heat model, a dynamic optimization model for heat exchanger network design in dynamic batch processes. To the best of our knowledge, the Dyn2Heat model is the first heat exchanger network design model to regard dynamics of batch processes in detail while addressing the trade-off between investment costs for heat exchangers, utility costs and the process duration. We

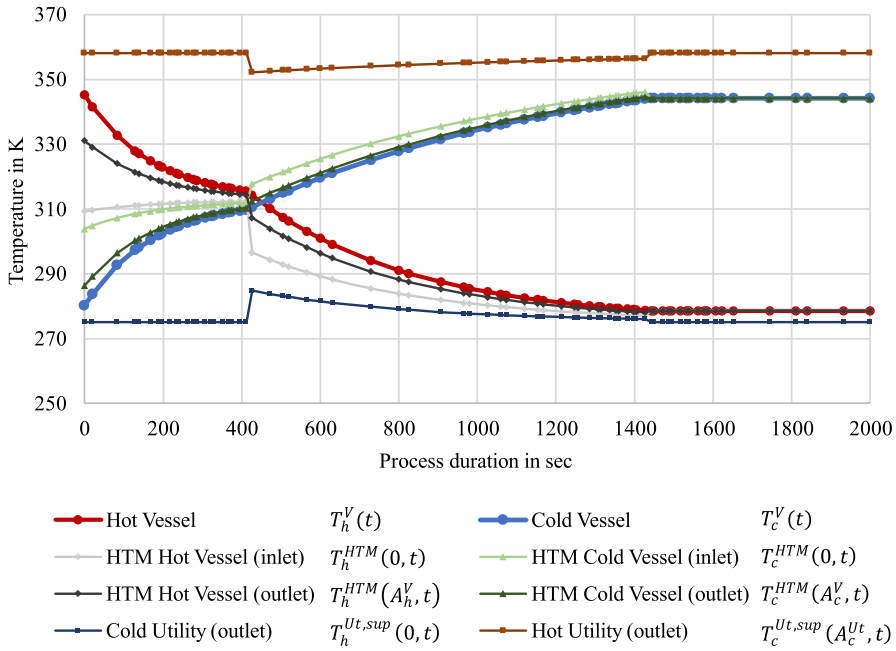


Fig. 8. Temporal temperature progression of the different fluids for the complex case study. The plot shows the following temperatures: the vessel temperatures $\boldsymbol{T_h^V}(t)$ and $\boldsymbol{T_c^V}(t)$, the temperature of the heat transfer medium in the hot vessel at the inlet of the vessel heat exchanger $\boldsymbol{T_h^{HTM}}(0,t)$ and at the outlet of the vessel heat exchanger $\boldsymbol{T_h^{HTM}}(A_h^V,t)$, the temperature of the heat transfer medium in the cold vessel at the inlet of the vessel heat exchanger $\boldsymbol{T_c^{HTM}}(0,t)$ and at the outlet of the vessel heat exchanger $\boldsymbol{T_c^{HTM}}(A_c^V,t)$, and the temperatures of the external utilities at the outlet of the utilities heat exchangers $\boldsymbol{T_h^{Ut,sup}}(0,t)$ and $\boldsymbol{T_c^{Ut,sup}}(A_c^{Ut},t)$.

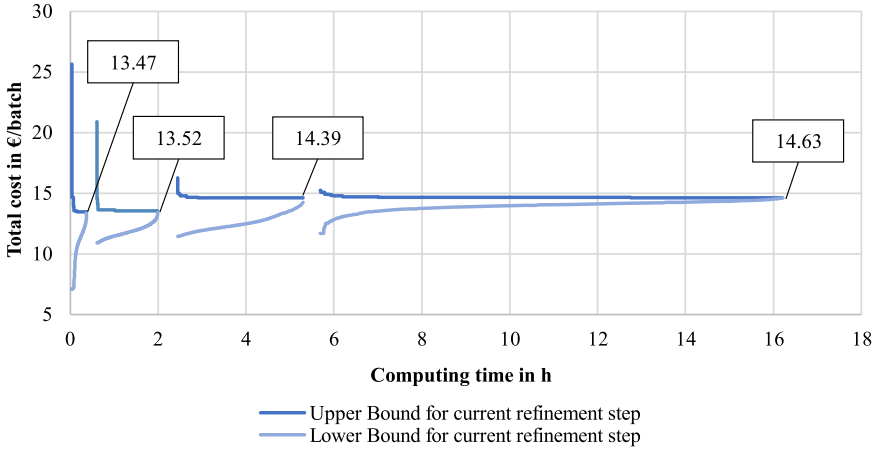


Fig. 9. Upper bounds and lower bounds plotted against the computing time for the complex case study. The upper and lower bound for each individual refinement step are shown one after the other. The optimal objective function value for each refinement step is given in the rectangles.

conclude that the Dyn2Heat model is a valuable supporting tool for the heat exchanger network design for batch processes.

We solve the Dyn2Heat model by direct transcription based on orthogonal collocation. By the direct transcription, the Dyn2Heat model becomes an MILP problem which is computationally efficient to solve by off-the-shelf solvers. We compare the Dyn2Heat model to algebraic optimization models based on the LMTD function in a small case study. In our comparison, the Dyn2Heat model reaches a similar solution quality while outperforming the algebraic optimization models regarding the computational effort. We conclude that the dynamic formulation is well suited to efficiently model two complexities in heat exchanger network design problems: temporal dynamics of batch processes and the nonlinear spatial temperature progression in heat exchangers. In a second case study, we show that the Dyn2Heat model can solve the design task also for more complex problems. Although the necessary computing time increases in comparison to the small case study, the computing time of the Dyn2Heat model is still acceptable for a design problem. Furthermore, first good solutions can be obtained very quickly also for more complex settings with a coarse resolution in the discretization. In comparison, the algebraic benchmark model based on the Chen approximation could not find a feasible solution within 24 h allowed computing time. The comparison underlines the superiority of the dynamic Dyn2Heat formulation.

The computational effort to solve the Dyn2Heat model, strongly depends on the accuracy of the discretization. The selection of discretization points leaves room for adjustment of the accuracy and the computational performance of the Dyn2Heat model. To address this trade-off, we propose an iterative refinement method to reach high accuracy in the discretization while keeping the computational effort low. In this work, we chose the discretization steps for the iterative refinement method manually. In future works, the computational efficiency could be further improved by introducing sophisticated rules for the

automated selection of the discretization steps in the refinement method.

One limitation of the Dyn2Heat model is the neglection of the heat exchanger transient behaviour. Under this assumption, the Dyn2Heat model is well suited to guide design decisions for heat exchangers in dynamic systems. To develop detailed control strategies for the heat integrated process and to perform a detailed heat exchanger design, dedicated methods should be used subsequently to the Dyn2Heat optimization.

In future works, it would be interesting to apply the Dyn2Heat model to bigger real-world systems. Due to its modular structure, the presented Dyn2Heat model offers the opportunity to be integrated into existing optimization models. For example, it would be beneficial to implement the dynamic Dyn2Heat formulation into existing generalized superstructure models for heat exchanger network design, like the Synheat model (Yee and Grossmann, 1990). This would allow to consider dynamic processes alongside stationary processes. Furthermore, the Dyn2Heat model could be adapted to superstructures including not only one-by-one matches, but allowing for the connection of one vessel with two or more.

Another valuable extension of the presented Dyn2Heat model is the modelling of isothermal streams, e.g., isothermal reactions or phase changes. To include these in the Dyn2Heat model, the enthalpy model for idealized fluids ($\dot{m}\cdot c_p\cdot\Delta T$) would need to be replaced by a generalized enthalpy model including multiple phases, phase changes, and reactions in the respective constraints. All in all, we conclude that the Dyn2Heat model opens the door for a detailed consideration of dynamic batch processes in heat exchanger network design problems.

Nomenclature

Sets of the Dyn2Heat Model:

Symbol	Description	Type
$a_m^{HI} \in [0 : a^{Max}]$	Area domain for external heat exchanger	continuous
$a_c^{Ut} \in [0 : a^{Max}]$	Area domain for utility supply in cold vessel	continuous
$a_h^{Ut} \in [0 : a^{Max}]$	Area domain for utility supply in hot vessel	continuous
$a_c^{V} \in [0 : a^{Max}]$	Area domain for heat transfer between cold vessel fluid and heat transfer medium	continuous
$a_h^{V} \in [0 : a^{Max}]$	Area domain for heat transfer between hot vessel fluid and heat transfer medium	continuous
$c \in C$	Cold vessels (heating demand)	discrete
$h \in H$	Hot vessels (cooling demand)	discrete
$m \in M$	Match of a hot and a cold vessel	discrete
$t \in [0 : t^{Max}]$	Time domain	continuous

Variables of the Dyn2Heat Model:

Symbol	Unit	Description
A_m^{HI}	m^2	Heat exchanger area of external heat exchanger for match m
A_h^{Ut}	m^2	Heat exchanger area for cold utility supply for hot vessel h
A_c^{Ut}	m^2	Heat exchanger area for hot utility supply for cold vessel c
A_h^{V}	m^2	Heat exchanger area for hot vessel h
A_c^{V}	m^2	Heat exchanger area for cold vessel c
$cost^{invest,total}$	$€/year$	Total annualized investment costs for all heat exchangers
$cost^{operational,total}$	$€/batch$	Total operational costs for one batch run
dur	s	Overall process duration
dur^{HI}	s	Duration of heat integration
dur_c^{Ut}	s	Duration of hot utility supply for cold vessel c
dur_h^{Ut}	s	Duration of cold utility supply for hot vessel h
Q_c^{Ut}	kJ	Heat supplied by hot utility for cold vessel c
Q_h^{Ut}	kJ	Heat supplied by cold utility for hot vessel h

(continued on next column)

(continued)

Symbol	Unit	Description
$T_m^{HI,cold}(a_m^{HI},t)$	K	Local, current temperature of heat transfer medium at the cold side of the external heat exchanger for match m
$T_m^{HI,hot}(a_m^{HI},t)$	K	Local, current temperature of heat transfer medium at the hot side of the external heat exchanger for match m
$T_c^{HTM}(a_c^{V},t)$	K	Local, current temperature of heat transfer medium in heat exchanger of cold vessel c
$T_h^{HTM}(a_h^{V},t)$	K	Local, current temperature of heat transfer medium in heat exchanger of hot vessel h
$T_c^{Ut}(a_c^{Ut},t)$	K	Local, current temperature of hot utility for cold vessel supply c
$T_h^{Ut}(a_h^{Ut},t)$	K	Local, current temperature of cold utility for hot vessel supply h
$T_c^{V}(t)$	K	Current temperature of fluid in hot vessel c
$T_h^{V}(t)$	K	Current temperature of fluid in hot vessel h or cold vessel c
$x_m^{HI}(a_m^{HI})$	–	Binary to decide on size of external heat exchanger for match m
$x_m^{t,HI}(t)$	–	Binary to decide on duration of heat integration for match m
$x_c^{t,Ut}(t)$	–	Binary to decide on duration of hot utility supply for cold vessel c
$x_h^{t,Ut}(t)$	–	Binary to decide on duration of cold utility supply for hot vessel h
$x_h^{Ut}(a_h^{Ut})$	–	Binary to decide on size of heat exchanger for cold utility supply for hot vessel h
$x_c^{Ut}(a_c^{Ut})$	–	Binary to decide on size of heat exchanger for hot utility supply for cold vessel c
$x_h^{V}(a_h^{V})$	–	Binary to decide on size of heat exchanger in hot vessel h
$x_c^{V}(a_c^{V})$	–	Binary to decide on size of heat exchanger in cold vessel c

Parameters of the Dyn2Heat Model:

Symbol	Unit	Description
$c_{p,c}$	$\frac{kJ}{kg\ K}$	Specific heat capacity of fluid in cold vessel c
$c_{p,h}$	$\frac{kJ}{kg\ K}$	Specific heat capacity of fluid in hot vessel h
$c_{p,m}^{HI,cold}$	$\frac{kJ}{kg\ K}$	Specific heat capacity of heat transfer medium at the cold side of the external heat exchanger for match m
$c_{p,m}^{HI,hot}$	$\frac{kJ}{kg\ K}$	Specific heat capacity of heat transfer medium at the hot side of the external heat exchanger for match m
$c_{p,h}^{HTM}$	$\frac{kJ}{kg\ K}$	Specific heat capacity of heat transfer medium in hot vessel h
$c_{p,c}^{HTM}$	$\frac{kJ}{kg\ K}$	Specific heat capacity of heat transfer medium in cold vessel c
$c_{p,c}^{Ut}$	$\frac{kJ}{kg\ K}$	Specific heat capacity of hot utility for cold vessel c
$c_{p,h}^{Ut}$	$\frac{kJ}{kg\ K}$	Specific heat capacity of cold utility for hot vessel h
$cost^{HEX,A}$	$\frac{€}{m^2}$	Specific investment costs for all heat exchangers
$cost^{HEX,init}$	$€$	Initial investment costs for all heat exchangers
$cost^{t}$	$\frac{€}{s}$	Specific time costs
$cost_c^{Ut}$	$\frac{€}{kJ}$	Specific costs of hot external utility to supply cold vessel c
$cost_h^{Ut}$	$\frac{€}{kJ}$	Specific costs of cold external utility to supply hot vessel h
k	$\frac{W}{m^2\ K}$	Heat transfer coefficient for all heat exchangers
M	–	Big-M parameter
$\dot{m}_m^{HI,cold}$	$\frac{kg}{s}$	Massflow of heat transfer medium at the cold side of the external heat exchanger for match m
$\dot{m}_m^{HI,hot}$	$\frac{kg}{s}$	Massflow of heat transfer medium at the hot side of the external heat exchanger for match m
$\dot{m}_c^{HTM}$	$\frac{kg}{s}$	Massflow of heat transfer medium connected to hot vessel c
$\dot{m}_h^{HTM}$	$\frac{kg}{s}$	Massflow of heat transfer medium connected to hot vessel h
$\dot{m}_c^{Ut}$	$\frac{kg}{s}$	Mass flow of hot utility for cold vessel c

(continued on next page)

(*continued*)

Symbol	Unit	Description
$\dot{m}_h^{Ut}$	$\frac{kg}{s}$	Mass flow of cold utility for hot vessel h
m_c^V	kg	Mass of fluid in cold vessel c
m_h^V	kg	Mass of fluid in hot vessel h
N^b	–	Number of batches per year
$T_c^{Ut,sup,0}$	K	Inlet temperature of hot utility for cold vessel c
$T_h^{Ut,sup,0}$	K	Inlet temperature cold utility for hot vessel h
$T_c^{V,start}$	K	Start temperature of cold vessel c
$T_h^{V,start}$	K	Start temperature of hot vessel h
$T_c^{V,target}$	K	Target temperature of cold vessel c
$T_h^{V,target}$	K	Target temperature of hot vessel h

Additional Variables of the Algebraic Benchmark Model:

Symbol	Unit	Description
$LMTD^{area,t0}$	K	Spatial logarithmic mean temperature difference at the beginning of the process
$LMTD^{area,t^{HI}}$	K	Spatial logarithmic mean temperature difference after heat integration
$LMTD^{time}$	K	Temporal logarithmic mean temperature difference at the hot end of the external heat exchanger
$LMTD^{total}$	K	Total double logarithmic mean temperature difference over time and area of the external heat exchanger

Appendix A

Discussion on the validity of assuming quasi steady-state behaviour of the heat exchangers

The assumption of quasi steady-state behaviour of the heat exchangers is valid if the dynamics of the surrounding system are slow in comparison to the transient response of the heat exchangers.

The surrounding system is mainly characterized by the dynamics of the vessel temperatures. While the dynamics of the heat exchanger are in the order of magnitude of the dwell time of a fluid particle in the heat exchanger, the dynamics of the surrounding system are present on a larger time scale, namely the process duration. As a measure of this relation, we introduce a dimensionless number that relates the heat capacity flow rate of the HTM ($\dot{m}^{HTM} \cdot c_p^{HTM}$) multiplied by the dwell time of the fluid in the heat exchanger Δt_d to the heat capacity of the connected vessels ($m^V c_p^V$):

$$\frac{\dot{m}^{HTM} \cdot c_p^{HTM} \cdot \Delta t_d}{m^V \cdot c_p^V}$$

If this dimensionless number is small (i.e. $<< 1$), the change in inlet temperature will only be small in comparison to the temperature change of a fluid particle travelling through the heat exchanger in the same time period which justifies the neglection of the temporal derivative in equation (1).

The dwell time can be expressed as:

$$\Delta t_d = \frac{L}{v} = \frac{A \cdot \rho \cdot S}{a \cdot c_p^{HTM}}$$

The ratio equals half the tube radius for tubes and the height of the flow channel for plates. With an assumed ratio $\frac{S}{a}$ of 1 cm, and a density of milk of 1000 $\frac{kg}{m^3}$, the proposed measure leads to

$$\frac{3.9\ \frac{kJ}{kg \cdot K} \cdot 7.5\ m^2 \cdot 1000 \frac{kg}{m^3} \cdot 0.01 m}{3.9 \frac{kJ}{kg \cdot K} \cdot 1000\ kg} = 0.075$$

for the cold side of the heat exchanger in the first case study. This value can be interpreted as the temperature change of the vessel related to the mean temperature change along the heat exchanger during the dwell time. We conclude that the assumption of quasi steady-state behaviour is reasonable for the case study in this work.

Another aspect to consider is the transient behaviour of the heat exchanger. By neglecting the thermal capacity and the thermal inertia of the heat exchanger walls, the transient behaviour is predominated by the propagation of the transient front through the heat exchanger. The lag time, which describes the time lag from the timepoint when the input temperature changes to the first change in the outlet temperature, is mainly influenced by the fluid velocity (Bobič et al., 2020). Thus, a high mass flow rate of the fluids in the heat exchanger leads to fast transient behaviour.

To further validate the model assumption, we set up a simulation model in the TIL library in Modelica (TLK Energy, 2023). We adapt the setup of the simulation model to the setup of the simplified case study. The modeled heat exchanger is a tube-and-tube counter-current heat exchanger with a tube diameter of 1cm and 10 parallel tubes. We use 640 cells to discretize a maximal heat exchanger area of 100 m^2. To compare the simulation model to the Dyn2Heat model, we solve the Dyn2Heat model for different parameter variations and use the results as parametrization for the simulation model. For a variation in the mass flow rates between 10 $\frac{kg}{s}$ and 40 $\frac{kg}{s}$, the deviation in the final vessel temperatures between the simulation results and the Dyn2Heat solution was found to be smaller than 0.6 %. The simulation model could also proof that the influence of the heat exchanger wall is negligible for the simulation results.

In conclusion, the assumption of quasi steady-state behaviour in the heat exchangers is valid for high heat capacities of the vessels in comparison to the heat capacity flow rates multiplied by the dwell time in the heat exchanger, neglectable thermal capacity and thermal inertia of the heat exchanger walls and fast fluid velocities in the heat exchangers, which implies a sufficiently small ratio of $\frac{S}{a}$.

Note that we also neglect the transients of the heat exchanger for the beginning of the heat exchange and for the switch of the operation mode from heat integration to utility supply. However, the Dyn2Heat model is well suited to guide design decisions for heat exchangers in dynamic systems. To develop detailed control strategies for the heat integrated process and to perform a detailed heat exchanger design, dedicated methods should be used subsequently to the Dyn2Heat optimization.

Appendix B

Complete Model Definition of the Dyn2Heat Optimization Model

Objective function:

$$\min_{\{\boldsymbol{A}_m^{HI},\ \boldsymbol{Q}_c^{Ut},\ \boldsymbol{Q}_h^{Ut},\ \boldsymbol{dur}\}} f\left(\boldsymbol{A}_m^{HI},\ \boldsymbol{Q}_c^{Ut}, \boldsymbol{Q}_h^{Ut}, \boldsymbol{dur}\right) = \frac{\boldsymbol{cost}^{\boldsymbol{invest},\ \boldsymbol{total}}}{N^{batch}} + \boldsymbol{cost}^{\boldsymbol{operation},\ \boldsymbol{total}} \tag{B1}$$

Operational cost:

$$\boldsymbol{cost}^{\boldsymbol{operation},\ \boldsymbol{total}} = \sum_{c \in C} cost_c^{Ut} \cdot \boldsymbol{Q}_c^{Ut} + \sum_{h \in H} cost_h^{Ut} \cdot \boldsymbol{Q}_h^{Ut} + cost^{time} \cdot \boldsymbol{dur} \tag{B2}$$

Investment costs for heat exchangers:

$$\begin{aligned} &\boldsymbol{cost}^{\boldsymbol{invest},\ \boldsymbol{total}} \\ &= cost^{HEX,init} \cdot \left(\sum_{m \in M} (\boldsymbol{x}_m^{HI}(0) + \sum_{h \in H} (\boldsymbol{x}_h^V(0) + \boldsymbol{x}_h^{Ut}(0)) + \sum_{c \in C} (\boldsymbol{x}_c^V(0) + \boldsymbol{x}_c^{Ut}(0)) \right) \\ &\quad + cost^{HEX,A} \cdot \left(\sum_{m \in M} \boldsymbol{A}_m^{HI} + \sum_{h \in H} (\boldsymbol{A}_h^{Ut} + \boldsymbol{A}_h^V) + \sum_{c \in C} (\boldsymbol{A}_c^{Ut} + \boldsymbol{A}_c^V) \right) \end{aligned} \tag{B3}$$

External Heat Exchangers:

$$\dot{m}_{m}^{HI,cold}\cdot c_{p,m}^{HI,cold}\cdot\frac{dT_{m}^{HI,cold}\left(a_{m}^{HI},t\right)}{da_{m}^{HI}} = x_{m}^{HI}\left(a_{m}^{HI}\right)\cdot x_{m}^{t,HI}(t)\cdot k\cdot\left(T_{m}^{HI,cold}\left(a_{m}^{HI},t\right)-T_{m}^{HI,hot}\left(a_{m}^{HI},t\right)\right)\ \forall m\in M \tag{B4}$$

$$\dot{m}_{m}^{HI,hot}\cdot c_{p,m}^{HI,hot}\cdot\frac{dT_{m}^{HI,hot}\left(a_{m}^{HI},t\right)}{da_{m}^{HI}} = x_{m}^{HI}\left(a_{m}^{HI}\right)\cdot x_{m}^{t,HI}(t)\cdot k\cdot\left(T_{m}^{HI,cold}\left(a_{m}^{HI},t\right)-T_{m}^{HI,hot}\left(a_{m}^{HI},t\right)\right)\ \forall\, m\in M \tag{B5}$$

The constraints are linearized by a big-M formulation as given in Eq. (6a)-(6f).

Vessels:

$$\dot{m}_{h}^{HTM}\cdot c_{p,h}^{HTM}\cdot\frac{dT_{h}^{HTM}\left(a_{h}^{V},t\right)}{da_{h}^{V}} = x_{h}^{V}\left(a_{h}^{V}\right)\cdot x_{h}^{t,Ut}(t)\cdot k\cdot\left(T_{h}^{V}(t)-T_{h}^{HTM}\left(a_{h}^{V},t\right)\right)\ \forall\, h\in H \tag{B6}$$

$$\dot{m}_{c}^{HTM}\cdot c_{p,c}^{HTM}\cdot\frac{dT_{c}^{HTM}\left(a_{c}^{V},t\right)}{da_{c}^{V}} = x_{c}^{V}\left(a_{c}^{V}\right)\cdot x_{c}^{t,Ut}(t)\cdot k\cdot\left(T_{c}^{V}(t)-T_{c}^{HTM}\left(a_{c}^{V},t\right)\right)\ \forall\, c\in C \tag{B7}$$

The constraints are linearized by a big-M formulation analogously to Eq.(6a).

$$m_{c}^{V}\cdot c_{p,c}^{V}\cdot\frac{dT_{c}^{V}(t)}{dt} = \dot{m}_{c}^{HTM}\cdot c_{p,c}^{HTM}\cdot\left(T_{c}^{HTM}\left(a_{c}^{V}=0,\ t\right)-T_{c}^{HTM}\left(a_{c}^{V}=A_{c}^{V},\ t\right)\right)\ \forall c\in C \tag{B8}$$

$$m_{h}^{V}\cdot c_{p,h}^{V}\cdot\frac{dT_{h}^{V}(t)}{dt} = \dot{m}_{h}^{HTM}\cdot c_{p,h}^{HTM}\cdot\left(T_{h}^{HTM}\left(a_{h}^{V}=0,\ t\right)-T_{h}^{HTM}\left(a_{h}^{V}=A_{h}^{V},\ t\right)\right)\ \forall h\in H \tag{B9}$$

Starting condition for cold vessel:

$$T_{c}^{V}(t=0) = T_{c}^{V,start}\qquad \forall c\in C \tag{B10}$$

Starting condition for hot vessel:

$$T_{h}^{V}(t=0) = T_{h}^{V,start}\qquad \forall h\in H \tag{B11}$$

Target conditions for the vessel temperatures. The parameter ε^{target} introduces a small slack to the final temperatures to improve the computational performance.

$$T_{h}^{V}(t=t^{max}) \le T_{h}^{V,target}+\varepsilon^{target}\qquad \forall h\in H \tag{B12}$$

$$T_{c}^{V}(t=t^{max}) \ge T_{c}^{V,target}-\varepsilon^{target}\qquad \forall c\in C \tag{B13}$$

Binaries for utility supply cannot be switched off before target temperatures are reached:

$$T_{h}^{V}(t)-T_{h}^{V,target} \le x_{h}^{t,Ut}(t)\cdot M+\varepsilon^{target}\qquad \forall h\in H \tag{B14a}$$

$$T_{h}^{V}(t)-T_{h}^{V,target} \ge -x_{h}^{t,Ut}(t)\cdot M-\varepsilon^{target}\qquad \forall h\in H \tag{B14b}$$

$$T_{c}^{V}(t)-T_{c}^{V,target} \le x_{c}^{t,Ut}(t)\cdot M+\varepsilon^{target}\qquad \forall c\in C \tag{B14c}$$

$$T_{c}^{V}(t)-T_{c}^{V,target} \ge -x_{c}^{t,Ut}(t)\cdot M-\varepsilon^{target}\qquad \forall c\in C \tag{B14d}$$

Set temperatures in vessel heat exchangers to vessel temperature, after utility supply is turned off:

$$T_{h}^{HTM}\left(A_{h}^{V,max},t\right)-T_{h}^{V}(t) \le x_{h}^{t,Ut}(t)\cdot M\qquad \forall h\in H \tag{B15a}$$

$$T_{h}^{HTM,}\left(A_{h}^{V,max},t\right)-T_{h}^{V}(t) \ge -x_{h}^{t,Ut}\ (t)\cdot M\qquad \forall h\in H \tag{B15b}$$

$$T_{c}^{HTM}\left(A_{c}^{V,max},t\right)-T_{c}^{V}(t) \le x_{c}^{t,Ut}(t)\cdot M\qquad \forall c\in C \tag{B15c}$$

$$T_{c}^{HTM}\left(A_{c}^{V,max},t\right)-T_{c}^{V}(t) \ge -x_{c}^{t,Ut}(t)\cdot M\qquad \forall c\in C \tag{B15d}$$

Utility Supply:

$$\dot{m}_{c}^{HTM}\cdot c_{p,c}^{HTM}\cdot\frac{dT_{c}^{Ut}\left(a_{c}^{Ut},t\right)}{da_{c}^{Ut}} = x_{c}^{Ut}\left(a_{c}^{Ut}\right)\cdot\left(1-x_{m_{c}}^{t,HI}(t)\right)\cdot x_{c}^{t,Ut}(t)\cdot k\cdot\left(T_{c}^{Ut}\left(a_{c}^{Ut},t\right)-T_{c}^{Ut,sup}\left(a_{c}^{Ut},t\right)\right)\ \forall\, c\in C \tag{B16}$$

$$\dot{m}_{c}^{Ut}\cdot c_{p,c}^{Ut}\cdot\frac{dT_{c}^{Ut,sup}\left(a_{c}^{Ut},t\right)}{da_{c}^{Ut}} = x_{c}^{Ut}\left(a_{c}^{Ut}\right)\cdot\left(1-x_{m_{c}}^{t,HI}(t)\right)\cdot x_{c}^{t,Ut}(t)\cdot k\cdot\left(T_{c}^{Ut}\left(a_{c}^{Ut},t\right)-T_{c}^{Ut,sup}\left(a_{c}^{Ut},t\right)\right)\ \forall c\in C \tag{B17}$$

$$\dot{m}_{h}^{HTM}\cdot c_{p,h}^{HTM}\cdot\frac{dT_{h}^{Ut}\left(a_{h}^{Ut},t\right)}{da_{h}^{Ut}} = x_{h}^{Ut}\left(a_{h}^{Ut}\right)\cdot\left(1-x_{m_{h}}^{t,HI}(t)\right)\cdot x_{h}^{t,Ut}(t)\cdot k\cdot\left(T_{h}^{Ut,sup}\left(a_{h}^{Ut},t\right)-T_{h}^{Ut}\left(a_{h}^{Ut},t\right)\right)\ \forall\, h\in H \tag{B18}$$

$$\dot{m}_{h}^{Ut}\cdot c_{p,h}^{Ut}\cdot\frac{dT_{h}^{Ut,sup}\left(a_{h}^{Ut},t\right)}{da_{h}^{Ut}} = x_{h}^{Ut}\left(a_{h}^{Ut}\right)\cdot\left(1-x_{m_{h}}^{t,HI}(t)\right)\cdot x_{h}^{t,Ut}(t)\cdot k\cdot\left(T_{h}^{Ut,sup}\left(a_{h}^{Ut},t\right)-T_{h}^{Ut}\left(a_{h}^{Ut},t\right)\right)\ \forall\, h\in H \tag{B19}$$

The constraints are linearized by a big-M formulation analogously to Eq. (6a).

The inlet temperatures of the utilities are predefined as constant parameters:

$$T_{h}^{Ut,sup}\left(A_{h}^{Ut,max},\ t\right) = T_{h}^{Ut,sup,0}\qquad \forall\, h\in\ H \tag{B20}$$

$$T_{c}^{Ut,sup}(0,\ t) = T_{c}^{Ut,sup,0}\qquad \forall c\in C \tag{B21}$$

The overall utility demand for a hot vessel Q_{h}^{CU} and a cold vessel Q_{c}^{HU}:

$$Q_{h}^{Ut} = \int_{t\in time}\dot{m}_{h}^{Ut}\cdot c_{p,h}^{Ut}\cdot\left(T_{h}^{Ut,sup}\left(a_{h}^{Ut}=0,t\right)-T_{h}^{Ut,sup}\left(A_{h}^{Ut,\max},t\right)\right)\ \forall\, h\in H \tag{B22}$$

$$Q_{c}^{Ut} = \int_{t\in time}\dot{m}_{c}^{Ut}\cdot c_{p,c}^{Ut}\cdot\left(T_{c}^{Ut,sup}\left(a_{c}^{Ut}=0,t\right)-T_{c}^{Ut,sup}\left(A_{c}^{Ut,\max},t\right)\right)\ \forall\, c\in C \tag{B23}$$

Derive optimal heat exchanger surface areas and optimal duration:

$$A_{m}^{HI} \ge x_{m}^{HI}\left(a_{m}^{HI}\right)\cdot a_{m}^{HI}\qquad \forall m\in M \tag{B24a}$$

$$A_{h}^{Ut} \ge x_{h}^{Ut}\left(a_{h}^{Ut}\right)\cdot a_{h}^{Ut}\qquad \forall h\in H \tag{B24b}$$

$$\boldsymbol{A_c^{Ut}} \geq \boldsymbol{x_c^{Ut}}\left(a_c^{Ut}\right)\cdot a_c^{Ut} \quad \forall c \in C \tag{B24c}$$

$$\boldsymbol{A_h^{V}} \geq \boldsymbol{x_h^{V}}\left(a_h^{V}\right)\cdot a_h^{V} \quad \forall h \in H \tag{B24d}$$

$$\boldsymbol{A_c^{V}} \geq \boldsymbol{x_c^{V}}\left(a_c^{V}\right)\cdot a_c^{V} \quad \forall c \in C \tag{B24e}$$

$$\boldsymbol{dur_m^{HI}} \geq \boldsymbol{x_m^{t,HI}}(t)\cdot t \quad \forall m \in M \tag{B24f}$$

$$\boldsymbol{dur_h^{Ut}} \geq \boldsymbol{x_h^{t,Ut}}(t)\cdot t \quad \forall h \in H \tag{B24g}$$

$$\boldsymbol{dur_c^{Ut}} \geq \boldsymbol{x_c^{t,Ut}}(t)\cdot t \quad \forall c \in C \tag{B24h}$$

$$\boldsymbol{dur} \geq \boldsymbol{dur_c^{Ut}} \quad \forall c \in C \tag{B24i}$$

$$\boldsymbol{dur} \geq \boldsymbol{dur_h^{Ut}} \quad \forall h \in H \tag{B24j}$$

The following continuity constraints guarantee that contiguous areas and durations are used, instead of splitting the area or duration to several separate parts. The split could otherwise occur due to the non-equidistant distribution of the discretization points.

$$\boldsymbol{x_m^{HI}}\left(a_m^{HI}\right) \geq \boldsymbol{x_m^{HI}}\left(a_m^{HI'}\right) \quad \textit{with } a_m^{HI} \leq a_m^{HI'} \quad \forall m \in M \tag{B25a}$$

$$\boldsymbol{x_c^{V}}\left(a_c^{V}\right) \geq \boldsymbol{x_c^{V}}\left(a_c^{V}\right) \quad \textit{with } a_c^{V} \leq a_c^{V} \quad \forall c \in C \tag{B25b}$$

$$\boldsymbol{x_h^{V}}\left(a_h^{V}\right) \geq \boldsymbol{x_h^{V}}\left(a_h^{V}\right) \quad \textit{with } a_h^{V} \leq a_h^{V} \quad \forall h \in H \tag{B25c}$$

$$\boldsymbol{x_c^{Ut}}\left(a_c^{Ut}\right) \geq \boldsymbol{x_c^{Ut}}\left(a_c^{Ut}\right) \quad \textit{with } a_c^{Ut} \leq a_c^{Ut} \quad \forall c \in C \tag{B25d}$$

$$\boldsymbol{x_h^{Ut}}\left(a_h^{Ut}\right) \geq \boldsymbol{x_h^{Ut}}\left(a_h^{Ut}\right) \quad \textit{with } a_h^{Ut} \leq a_h^{Ut} \quad \forall h \in H \tag{B25e}$$

$$\boldsymbol{x_m^{t,HI}}(t) \geq \boldsymbol{x_m^{t,HI}}(t') \quad \textit{with } t \leq t' \quad \forall m \in M \tag{B25f}$$

$$\boldsymbol{x_h^{t,Ut}}(t) \geq \boldsymbol{x_h^{t,Ut}}(t') \quad \textit{with } t \leq t' \quad \forall h \in H \tag{B25g}$$

$$\boldsymbol{x_c^{t,Ut}}(t) \geq \boldsymbol{x_c^{t,Ut}}(t') \quad \textit{with } t \leq t' \quad \forall c \in C \tag{B25h}$$

Connect the temperatures between the heat exchangers (here exemplarily defined for the superstructure in Fig. 2):

$$\boldsymbol{T_h^{HTM}}\left(A_h^{V,max},t\right) = \boldsymbol{T_{m_h}^{HI}}(0,t) \tag{B26a}$$

$$\boldsymbol{T_{m_h}^{HI}}\left(A_h^{HI,max},t\right) = \boldsymbol{T_h^{Ut}}(0,t) \tag{B26b}$$

$$\boldsymbol{T_h^{Ut}}\left(A_h^{Ut,max},t\right) = \boldsymbol{T_h^{HTM}}(0,t) \tag{B26c}$$

$$\boldsymbol{T_c^{HTM}}\left(A_c^{V,max},t\right) = \boldsymbol{T_{m_c}^{HI}}\left(A_m^{HI,max},t\right) \tag{B26d}$$

$$\boldsymbol{T_{m_c}^{HI}}(0,t) = \boldsymbol{T_c^{Ut}}\left(A_c^{Ut,max},t\right) \tag{B26e}$$

$$\boldsymbol{T_c^{Ut}}(0,t) = \boldsymbol{T_c^{HTM}}(0,t) \tag{B26f}$$

To model the system structure given in Fig. 2, we assume that the external heat exchanger and the heat exchangers for utilities are placed in a row. The binaries switch the heat transfer on-/and off, i.e., they model a bypass.

The modular formulation of the heat exchangers and the connection of the temperatures allows to adapt the Dyn2Heat model to several superstructures, representing the predefined allowed matches $m \in M$. Note that, besides the temperatures, the mass flows $\dot{m}$ and heat capacities c_p of the fluids must match for connected streams. The mass flows and heat capacities are input parameters to the model and must be set accordingly when defining the system structure of the model.

Appendix C

Collocation Equation for the Dyn2Heat Model

In the following we derive the collocation equation exemplarily for the the temperature of the cold vessel $\boldsymbol{T_c^{V,K}}(t)$, based on (Biegler, 2010). The Lagrange polynomial is

$$T_c^{V,K}(t) = \sum_{j=0}^{K} l_j(\tau)\ T_{c,\ ij}^{V}$$

, where

$$l_{j(\tau)} = \prod_{k=0,\neq j}^{K} \frac{\tau - \tau_k}{\tau_j - \tau_k}$$

. τ is the normalized time over the finite element i of length h_i, i.e. $t = t_{i-1} + h_i\tau$ with $t \in [t_{i-1}, t_i]$ and $\tau \in [0,1]$.

$j = 0,\ \ldots,\ K-1$ are the collocation points and $\tau_0 = 0,\ \tau_j < \tau_{j+1}$.

Substituting the derivative of the Lagrange polynomial into Eq. (14) leads to the collocation equation:

$$\left.\frac{dT_c^{V,K}(t)}{dt}\right|_{t_{i,j}} = \frac{1}{h_i}\sum_{j=0}^{K} T_{c,ij}^{V}\frac{dl_j(\tau_k)}{d\tau} = \frac{\overset{HTM}{m}_c \cdot c_{p,c}^{HTM}}{m_c^{V}\cdot c_{p,c}^{V}}\cdot\left(T_c^{HTM}\left(a_c^{V}=0,\ t\right) - T_c^{HTM}\left(a_c^{V}=A_c^{V,max},\ t\right)\right)$$

Appendix D

Complete Model Definition of the Algebraic Benchmark Model

The objective function equals the objective function of the Dyn2Heat model:

$$\min_{\left\{\boldsymbol{A^{HI}},\boldsymbol{Q_c^{Ut}},\boldsymbol{Q_h^{Ut}},\boldsymbol{dur}\right\}} f\left(\boldsymbol{A^{HI}},\boldsymbol{Q_c^{Ut}},\boldsymbol{Q_h^{Ut}},\boldsymbol{dur}\right) = \frac{\boldsymbol{cost^{invest}}}{N^{batch}} + \boldsymbol{cost^{operation}} \tag{D1}$$

, with

$$\boldsymbol{cost^{invest,total}} = cost^{HEX,init}\cdot\boldsymbol{x^{HI}} + cost^{HEX,A}\cdot\boldsymbol{A^{HI}} \tag{D2}$$

and

$$\boldsymbol{cost^{operation,\ total}} = cost_c^{Ut}\cdot\boldsymbol{Q_c^{Ut}} + cost_h^{Ut}\cdot\boldsymbol{Q_h^{Ut}} + cost^{time}\cdot\boldsymbol{dur} \tag{D3}$$

The utility demands are defined as:

$$\boldsymbol{Q_c^{Ut}} = m_c^{V}\cdot c_{p,c}^{V}\cdot\left(T_c^{V,target} - \boldsymbol{T_c^{V}}\left(dur^{HI}\right)\right) \tag{D4}$$

$$\boldsymbol{Q_h^{Ut}} = m_h^{V}\cdot c_{p,h}^{V}\cdot\left(\boldsymbol{T_h^{V}}\left(dur^{HI}\right) - T_h^{V,target}\right) \tag{D5}$$

The integrated heat is:

$$\boldsymbol{Q^{HI}} = k\cdot\boldsymbol{A^{HI}}\cdot\boldsymbol{LMTD^{total}}\cdot\boldsymbol{dur^{HI}} \tag{D6}$$

and the optimal heat exchanger surface area can be derived from

$$k\cdot\boldsymbol{LMTD^{area,t0}}\cdot\boldsymbol{A^{HI}} = \dot{m}_c\cdot c_{p,c}\cdot\left(T^{HI,cold}(0,0) - T^{HI,cold}\left(\boldsymbol{A^{HI}},0\right)\right) \tag{D7}$$

$$k\cdot\boldsymbol{LMTD^{area,t0}}\cdot\boldsymbol{A^{HI}} = \dot{m}_h\cdot c_{p,h}\cdot\left(\boldsymbol{T^{HI,hot}}\left(A^{HI},0\right) - T^{HI,hot}(0,0)\right) \tag{D8}$$

$$k\cdot\boldsymbol{LMTD^{area,\ t^{HI}}}\cdot\boldsymbol{A^{HI}} = \dot{m}_c\cdot c_{p,c}\cdot\left(\boldsymbol{T^{HI,cold}}\left(0,dur^{HI}\right) - T^{HI,cold}\left(A^{HI},dur^{HI}\right)\right) \tag{D9}$$

$$k\cdot\boldsymbol{LMTD^{area,\ t^{HI}}}\cdot\boldsymbol{A^{HI}} = \dot{m}_h\cdot c_{p,h}\cdot\left(\boldsymbol{T^{HI,hot}}\left(A^{HI},dur^{HI}\right) - \boldsymbol{T^{HI,hot}}\left(0,dur^{HI}\right)\right) \tag{D10}$$

The overall heating and cooling demands (Q_h and Q_c) are supplied by external utilities ($\boldsymbol{Q_h^{Ut}}$ and $\boldsymbol{Q_c^{Ut}}$) and heat integration ($\boldsymbol{Q^{HI}}$).

$$Q_c = \boldsymbol{Q_c^{Ut}} + \boldsymbol{Q^{HI}} \tag{D11}$$

$$Q_h = \boldsymbol{Q_h^{Ut}} + \boldsymbol{Q^{HI}} \tag{D12}$$

The vessel temperatures after heat integration depend on the quantity of the integrated heat:

$$\boldsymbol{T_c^V}\left(dur^{HI}\right) = T_c^{V,start} + \frac{\boldsymbol{Q^{HI}}}{m_c^V \cdot c_{p,c}} \tag{D13}$$

$$\boldsymbol{T_h^V}\left(dur^{HI}\right) = T_h^{V,start} - \frac{\boldsymbol{Q^{HI}}}{m_h^V \cdot c_{p,h}} \tag{D14}$$

The double logarithmic mean temperature difference of the external heat exchanger is:

$$\boldsymbol{LMTD^{total}} = \frac{1}{T^{HI,hot}(0,\ 0) - \boldsymbol{T^{HI,cold}}(0,\ 0)} \cdot \boldsymbol{LMTD^{area,t0}} \cdot \boldsymbol{LMTD^{time}} \tag{D15}$$

with

$$\boldsymbol{LMTD^{time}} = \frac{\left(T^{HI,hot}(0,0) - \boldsymbol{T^{HI,cold}}(0,0)\right) - \left(\boldsymbol{T^{HI,hot}}(0,dur^{HI}) - \boldsymbol{T^{HI,cold}}(0,dur^{HI})\right)}{ln\left(\boldsymbol{T^{HI,hot}}(0,0) - \boldsymbol{T^{HI,cold}}(0,0)\right) - ln\left(\boldsymbol{T^{HI,hot}}(0,dur^{HI}) - \boldsymbol{T^{HI,cold}}(0,dur^{HI})\right)} \tag{D16}$$

and

$$\boldsymbol{LMTD^{area,t0}} = \frac{\left(T^{HI,hot}(0,\ 0) - \boldsymbol{T^{HI,cold}}(0,\ 0)\right) - \left(\boldsymbol{T^{HI,hot}}\left(A^{HI},\ 0\right) - T^{HI,cold}\left(A^{HI},\ 0\right)\right)}{ln\left(T^{HI,hot}(0,\ 0) - \boldsymbol{T^{HI,cold}}(0,\ 0)\right) - ln\left(\boldsymbol{T^{HI,hot}}\left(A^{HI},\ 0\right) - T^{HI,cold}\left(A^{HI},\ 0\right)\right)} \tag{D17}$$

The inlet temperatures of the heat exchanger equal the vessel temperatures at the start and finish of the heat integration

$$\boldsymbol{T^{HI,hot}}(0,0) = T_h^{V,start} \tag{D18}$$

$$\boldsymbol{T^{HI,cold}}\left(A^{HI},0\right) = T_c^{V,start} \tag{D19}$$

$$\boldsymbol{T^{HI,hot}}\left(0,dur^{HI}\right) = \boldsymbol{T_h^V}\left(dur^{HI}\right) \tag{D20}$$

$$\boldsymbol{T^{HI,cold}}\left(A^{HI},dur^{HI}\right) = \boldsymbol{T_c^V}\left(dur^{HI}\right) \tag{D21}$$

Note that all temperatures are only defined for discrete points (start and end of the process and inlet and outlet of the heat exchanger), instead for the whole continuous domains. To support the recognition, we have used the same symbols as in the Dyn2Heat model.

Appendix E

Parameters of both case studies:

Name	Symbol	Value	Unit	Reference
Mass of fluid in hot vessel	m_h^V	1000	kg	assumption
Mass of fluid cold vessel	m_c^V	1000	kg	assumption
Start temperature of hot vessel	$T_h^{V,start}$	345.15	K	(Fellows, 2017)
Target temperature of hot vessel	$T_h^{V,target}$	277.65	K	(Fellows, 2017)
Start temperature of cold vessel	$T_c^{V,start}$	280.15	K	(Fellows, 2017)
Target temperature of cold vessel	$T_c^{V,target}$	345.15	K	(Fellows, 2017)
Heat transfer coefficient for all heat exchangers	k	2800	$W\ m^{-2}\ K^{-1}$	(Fellows, 2017)
Specific costs of hot external utility	$cost_c^{Ut}$	3 E-5	$€\ kJ^{-1}$	assumption (oriented to a gas price of $100\frac{€}{MWh}$ (Statistisches Bundesamt 2023)
Specific costs of cold external utility	$cost_c^{Ut}$	3 E-6	$€\ kJ^{-1}$	assumption ($\frac{1}{10}$ of cost for hot utility)
Initial investment costs for all heat exchangers	$cost^{HEX,init}$	0	$€\ yr^{-1}$	assumption
Specific investment costs for all heat exchangers	$cost^{HEX,A}$	500	$€\ m^{-2}\ yr^{-1}$	assumption, oriented to (Escobar and Trierweiler, 2013)
Number of batches per year	N^b	8000	$batch\ yr^{-1}$	assumption

Additional parameters of the simplified case study:

Mass flow hot milk	$\dot{m}_h$	8	$kg\ s^{-1}$	assumption
Mass flow cold milk	$\dot{m}_c$	10	$kg\ s^{-1}$	assumption
Specific heat coefficient of hot and cold milk	$c_{p,h}$ and $c_{p,c}$	3.9	$kJ\ kg^{-1}\ K^{-1}$	(Fellows, 2017)
Specific time penalty	$cost^t$	0.01	$€\ s^{-1}$	assumption

Collocation parameters of the simplified case study:

Number of collocation points per finite element	3
Refinement step-width for time discretization in sec(in 5 iterative runs)	200; 100; 50; 30; 10
Refinement step-width for time discretization in m^2 (in 5 iterative runs)	20; 10; 5; 3; 1
Upper bound of area-axis (A^{max})	100 m^2
Upper bound of time-axis (t^{max})	1000 sec

Boundaries of finite elements in first and final run for simplified case study:

Discrete time steps of first run	0.000; 200.000; 400.000; 600.000; 800.000; 1000.000
Discrete time steps of final run	0.000; 64.495; 94.873; 112.758; 122.088; 131.418; 140.747; 150.077; 159.407; 168.737; 178.067; 205.798; 252.899; 300.000; 400.000; 600.000; 800.000; 1000.000
Discrete area steps of first run	0.000; 20.000; 40.000; 60.000; 80.000; 100.000
Discrete area steps of final run	0.000; 5.000; 7.080; 7.959; 8.838; 9.717; 10.596; 11.475; 12.354; 13.233; 14.112; 17.056; 20.000; 30.000; 40.000; 60.000; 80.000; 100.000

Additional parameters of the complex case study:

Name	Symbol	Value	Unit	Reference
Inlet temperature hot utility for cold vessel	$T_c^{Ut,sup,0}$	358,15	K	assumption
Inlet temperature cold utility for hot vessel	$T_h^{Ut,sup,0}$	277,65	K	assumption
Mass flow hot and cold utility	$\dot{m}_h^{Ut}$ and $\dot{m}_c^{Ut}$	9	$kg\ s^{-1}$	assumption
Slack parameter for target temperature	ϵ^{target}	1	K	assumption
Mass flow heat transfer medium (hot side)	$\dot{m}_h^{HTM} = \dot{m}_m^{HI,hot}$	8	$kg\ s^{-1}$	assumption
Mass flow heat transfer medium (cold side)	$\dot{m}_c^{HTM} = \dot{m}_m^{HI,cold}$	10	$kg\ s^{-1}$	assumption
Specific heat coefficient of both heat transfer media and hot and cold utility	$c_{p,c}^{HTM} = c_{p,m}^{HI,cold}$, $c_{p,h}^{HTM} = c_{p,m}^{HI,hot}$, $c_{p,h}^{Ut}$ and $c_{p,c}^{Ut}$	4.2	$kJ\ kg^{-1}\ K^{-1}$	assumption (oriented to water)
Specific time penalty	$cost^t$	0.005	$€\ s^{-1}$	assumption

Collocation parameters of the complex case study:

Number of collocation points per finite element	3
Refinement step-width for time discretization in *sec* (in 3 iterative runs)	400; 200; 100; 50
Refinement step-width for time discretization in m^2 (in 3 iterative runs)	6; 3; 2; 1
upper bound of all area-axis (A^{max})	30 m^2
upper bound of time-axis (t^{max})	2000 *sec*

Boundaries of finite elements in first and final run for simplified case study:

Discrete time steps of first run	0.000; 400.000; 800.000; 1200.000; 1600.000; 2000.000
Discrete time steps of final run	0.000; 128.990; 189.745; 234.115; 278.486; 322.856; 367.226; 411.596; 505.798; 600.000; 800.000; 966.384; 1060.064; 1153.745; 1247.426; 1307.845; 1352.895; 1397.944; 1442.994; 1488.043; 1533.093; 1578.142; 1623.192; 1811.596; 2000.000
Discrete area steps of first run for all areas	0.000; 6.000; 12.000; 18.000; 24.000; 30.000
Discrete area steps of final run for area A^{HI}	0.000; 2.496; 4.252; 6.009; 7.142; 8.009; 8.877; 9.745; 10.612; 11.480; 12.348; 15.174; 18.000; 24.000; 30.000
Discrete area steps of final run for area A_h^V	0.000; 6.000; 9.870; 11.045; 12.039; 13.033; 14.026; 15.020; 16.684; 18.348; 21.174; 24.000; 30.000
Discrete area steps of final run for area A_c^V	0.000; 6.000; 9.870; 12.696; 15.522; 18.348; 19.523; 20.439; 21.355; 22.271; 23.187; 24.102; 26.068; 28.034; 30.000
Discrete area steps of final run for area A_h^{Ut}	0.000; 3.000; 4.248; 5.092; 5.936; 6.780; 7.624; 8.467; 10.234; 12.000; 18.000; 24.000; 30.000
Discrete area steps of final run for area A_c^{Ut}	0.000; 1.000; 2.000; 3.000; 4.000; 6.000; 9.000; 12.000; 18.000; 24.000; 30.000

CRediT authorship contribution statement

Dörthe Franzisca Hagedorn: Writing – original draft, Visualization, Software, Project administration, Methodology, Investigation, Data curation, Conceptualization. **Laura Kuper:** Writing – review & editing, Visualization, Software, Methodology, Investigation, Data curation. **Mats Zoellmann:** Validation, Software, Methodology. **Christiane Reinert:** Writing – review & editing, Supervision. **Niklas von der Assen:** Writing – review & editing, Supervision, Funding acquisition, Conceptualization.

Declaration of competing interest

The authors declare that they have no known competing financial interests or personal relationships that could have appeared to influence the work reported in this paper.

Acknowledgements

This work was funded by the German Federal Ministry of Economic Affairs and Energy (ref. no.: 03EN2031D). We gratefully acknowledge the financial support.

We would like to thank Dr.-Ing. Florian Joseph Baader for the valuable discussions and his input during the development of the presented work, as well as Sören Demandt and Gereon Dohm for their valuable support.

Data availability

The original contributions presented in the study are included in the article, further inquiries can be directed to the corresponding author.

References

Aaltola, J., 2002. Simultaneous synthesis of flexible heat exchanger network. Appl Therm Eng 22 (8), 907–918. https://doi.org/10.1016/S1359-4311(02)00008-X.

Biegler, L.T., 2010. Nonlinear programming: Concepts, algorithms, and applications to chemical processes. Society for Industrial and Applied Mathematics.

Bobič, M., Gjerek, B., Golobič, I., Bajsić, I., 2020. Dynamic behaviour of a plate heat exchanger: Influence of temperature disturbances and flow configurations. International Journal of Heat and Mass Transfer 163, 120439. https://doi.org/10.1016/j.ijheatmasstransfer.2020.120439.

Boyadjiev, C., Ivanov, B., Vaklieva-Bancheva, N., Pantelides, C.C., Shah, N., 1996. Optimal energy integration in batch antibiotics manufacture. Comput Chem Eng 20, S31–S36. https://doi.org/10.1016/0098-1354(96)00016-6.

Castro, P.M., 2016. Improving Energy Efficiency in Batch Plants Through Direct Heat Integration. In: Martín, M.M. (Ed.), Alternative Energy Sources and Technologies. Springer International Publishing, Cham, pp. 341–362.

Chen, J., 1987. Comments on improvements on a replacement for the logarithmic mean. Chem Eng Sci 42 (10), 2488–2489. https://doi.org/10.1016/0009-2509(87)80128-8.

Chen, J., 2019. Logarithmic mean: Chen's approximation or explicit solution? Comput Chem Eng 120, 1–3. https://doi.org/10.1016/j.compchemeng.2018.10.002.
Dowidat, C., Ulonska, K., Bramsiepe, C., Schembecker, G., 2014. Heat integration in batch processes including heat streams with time dependent temperature progression. Appl Therm Eng 70 (1), 321–327. https://doi.org/10.1016/j.applthermaleng.2014.05.022.
Escobar, M., Trierweiler, J.O., 2013. Optimal heat exchanger network synthesis: A case study comparison. Appl Therm Eng 51 (1-2), 801–826. https://doi.org/10.1016/j.applthermaleng.2012.10.022.
Fellows, P., 2017. Food processing technology: Principles and practice. Woodhead Publishing, Duxford, United Kingdom.
Fernández, I., Renedo, C.J., Pérez, S.F., Ortiz, A., Mañana, M., 2012. A review: Energy recovery in batch processes. Renew Sust Energ Rev 16 (4), 2260–2277. https://doi.org/10.1016/j.rser.2012.01.017.
Fisher, R.C., 1944. Heating and Cooling Times in Circulating Systems. Ind Eng Chem 36 (10), 939–942. https://doi.org/10.1021/ie50418a017.
Glück, B., 2017. Bedeutung, detaillierte Herleitung und Berechnung der mittleren Temperaturdifferenz, der mittleren logarithmischen Temperaturdifferenz, der mittleren Stofftemperaturen (Medientemperaturen) und der Behälteraufheizzeiten bei der Wärmeübertragung zwischen stofflich getrennten Medien: Wärmeübertrager, Raumheizflächen, Behälteraufheizung. URL: <https://berndglueck.de/waermeuebertragung.php>. Accessed 26 October 2022.
Gurobi Optimization L.L.C., 2025. Gurobi Optimizer Reference Manual: Version 10.0. Gurobi Optimization L.L.C.
Hagedorn, D.F., Demandt, S., Baader, F.J., Reinert, C., Aßen, N.von der, 2023. DynHeat: Heat Exchanger Network Design for Batch Processes via Dynamic Optimization. In: Kokossis, A.C. (Ed.), 33rd European Symposium on Computer Aided Process Engineering: Escape-33, 1st ed. Elsevier, San Diego, pp. 2745–24750.
Hamze, S., Witrant, E., Bresch-Pietri, D., Fauvel, C., 2018. Estimating Heat-Transport and Time-Delays in a Heat Exchanger. 2018 IEEE Conference on Control Technology and Applications (CCTA): 21-24 Aug. 2018. IEEE, Piscataway, NJ, pp. 1514–1519, 2018 IEEE Conference on Control Technology and Applications (CCTA), Copenhagen. 8/21/2018 - 8/24/2018.
Huang, K.F., Al-mutairi, E.M., Karimi, I.A., 2012. Heat exchanger network synthesis using a stagewise superstructure with non-isothermal mixing. Chemical Engineering Science 73, 30–43. https://doi.org/10.1016/j.ces.2012.01.032.
Agency, International Energy, 2022. Renewables 2022: Analysis and forecast to 2027. IEA - International Energy Agency 159.
Ivanov, B., Peneva, K., Bancheva, N., 1992. Heat Integration of Batch Vessels At Fixed Time Interval I.: Schemes With Recycling Main Fluids. Hung J Ind Chem (Hungarian Journal of Industrial Chemistry) 20 (3), 225–231.
Kazi, S.R., Short, M., Biegler, L.T., 2021a. Heat exchanger network synthesis with detailed exchanger designs: Part 1. A discretized differential algebraic equation model for shell and tube heat exchanger design. AIChE J (1), 67. https://doi.org/10.1002/aic.17056.
Kazi, S.R., Short, M., Isafiade, A.J., Biegler, L.T., 2021b. Heat exchanger network synthesis with detailed exchanger designs—2. Hybrid optimization strategy for synthesis of heat exchanger networks. AIChE J (1), 67. https://doi.org/10.1002/aic.17057.
Kemp, I.C., Deakin, A.W., 1989a. The Cascade Analysis for Energy and Process Integration of Batch Processes, Part 1: Calculation of Energy Targets. Chem Eng Res Des 67, 495–509.
Kemp, I.C., Deakin, A.W., 1989b. The Cascade Analysis for Energy and Process Integration of Batch Processes, Part 2: Network Design and Process Scheduling. Chem Eng Res Des 67, 495–509.
Kemp, I.C., Lim, J.S., 2020. Pinch Analysis for Energy and Carbon Footprint Reduction: User Guide to Process Integration for the Efficient Use of Energy. Butterworth-Heinemann.
Klemeš, J.J., Kravanja, Z., 2013. Forty years of Heat Integration: Pinch Analysis (PA) and Mathematical Programming (MP). Curr Opin Chem Eng 2 (4), 461–474. https://doi.org/10.1016/j.coche.2013.10.003.
Linnhoff, B., Flower, J.R., 1978. Synthesis of heat exchanger networks: I. Systematic generation of energy optimal networks. AIChE J 24 (4), 633–642. https://doi.org/10.1002/aic.690240411.
Maidi, A., Diaf, M., Corriou, J.-P., 2009. Boundary geometric control of a counter-current heat exchanger. Journal of Process Control 19 (2), 297–313. https://doi.org/10.1016/j.jprocont.2008.03.002.
Mistry, M., Misener, R., 2016. Optimising heat exchanger network synthesis using convexity properties of the logarithmic mean temperature difference. Comput Chem Eng 94, 1–17. https://doi.org/10.1016/j.compchemeng.2016.07.001.
Nicholson, B., Siirola, J.D., Watson, J.-P., Zavala, V.M., Biegler, L.T., 2018. pyomo.dae: a modeling and automatic discretization framework for optimization with differential and algebraic equations. Math Prog Comp 10 (2), 187–223. https://doi.org/10.1007/s12532-017-0127-0.
Paterson, W.R., 1984. A replacement for the logarithmic mean. Chem Eng Sci 39 (11), 1635–1636. https://doi.org/10.1016/0009-2509(84)80090-1.
Peneva, K., Ivanov, B., Bancheva, N., 1992. Heat Integration of Batch Vessels at Fixed Time Interval II: Schemes With Intermediate Heating And Cooling Agents. Hung J Ind Chem (Hungarian Journal of Industrial Chemistry) 20 (3), 233–239.
Sahinidis, N., 2024. BARON 25.2.1. The Optimization Firm, LLC.
Sano, H., 2021. Stability analysis of heat exchangers with delayed boundary feedback. Automatica 127, 109540. https://doi.org/10.1016/j.automatica.2021.109540.
TLK Energy, 2023. Thermodynamik Simulation mit TIL Suite. URL: <https://tlk-energy.de/software/til-suite>. Accessed 6 June 2023.
Vaklieva-Bancheva, N.G., 2022. Chapter 5 - Energy Integration of Production Systems with Batch Processes in Chemical Engineering. In: Boyadjiev, C. (Ed.), Modeling and Simulation in Chemical Engineering. Springer International Publishing, Cham, pp. 101–125.
Vaselenak, J.A., Grossmann, I.E., Westerberg, A.W., 1986. Heat integration in batch processing. Ind. Eng. Chem. Proc. Des. Dev. 25 (2), 357–366. https://doi.org/10.1021/i200033a004.
Verheyen, W., Zhang, N., 2006. Design of flexible heat exchanger network for multi-period operation. Chem Eng Sci 61 (23), 7730–7753. https://doi.org/10.1016/j.ces.2006.08.043.
Yee, T.F., Grossmann, I.E., 1990. Simultaneous optimization models for heat integration—II. Heat exchanger network synthesis. Comput Chem Eng 14 (10), 1165–1184. https://doi.org/10.1016/0098-1354(90)85010-8.
Zhao, X.G., O'neill, B.K., Roach, J.R., Wood, R.M., 1998. Heat Integration For Batch Processes: Part 1: Process Scheduling Based on Cascade Analysis. Chem Eng Res Des 76 (6), 685–699. https://doi.org/10.1205/026387698525397.